This is an open access article published under an ACS AuthorChoice License, which permits copying and redistribution of the article or any adaptations for non-commercial purposes.

ACS Editors' Choice

ACS NANO

Cite This: ACS Nano 2019, 13, 9713−9734

www.acsnano.org

REVIEW

Recent Advances in Interface Engineering of Transition-Metal Dichalcogenides with Organic Molecules and Polymers

Kyungjune Cho,[†] Jinsu Pak,[†] Seungjun Chung,[*,‡] and Takhee Lee[*,†]

[†]Department of Physics and Astronomy and Institute of Applied Physics, Seoul National University, Seoul 08826, Korea
[‡]Photo-electronic Hybrids Research Center, Korea Institute of Science and Technology (KIST), Seoul 02792, Korea

ABSTRACT: The interface engineering of two-dimensional (2D) transition-metal dichalcogenides (TMDs) has been regarded as a promising strategy to modulate their outstanding electrical and optoelectronic properties because of their inherent 2D nature and large surface-to-volume ratio. In particular, introducing organic molecules and polymers directly onto the surface of TMDs has been explored to passivate the surface defects or achieve better interfacial properties with neighboring surfaces efficiently, thus leading to great opportunities for the realization of high-performance TMD-based applications. This review provides recent progress in the interface engineering of TMDs with organic molecules and polymers corresponding to the modulation of their electrical and optoelectronic characteristics. Depending on the interfaces between the surface of TMDs and dielectric, conductive contacts or the ambient environment, we present various strategies to introduce an organic interlayer from materials to processing. In addition, the role of native defects on the surface of TMDs, such as adatoms or vacancies, in determining their electrical characteristics is also discussed in detail. Finally, the future challenges and opportunities associated with the interface engineering are highlighted.

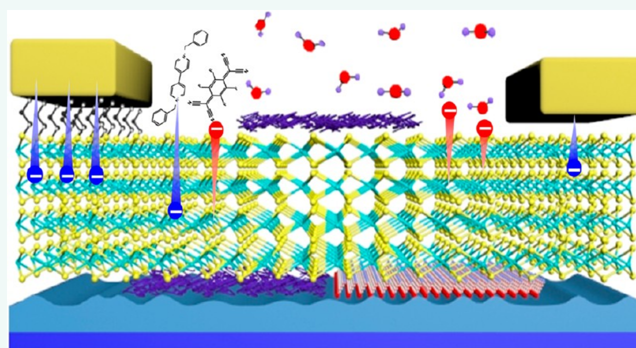

KEYWORDS: *two-dimensional materials, transition-metal dichalcogenides, surface engineering, interface engineering, contact engineering, molecular treatment, organic molecules, organic polymers, electric transport properties, charge injection properties*

In recent years, two-dimensional (2D) transition-metal dichalcogenides (TMDs), which are held together by weak van der Waals (vdW) interactions, have received much attention due to their tunable bandgap energy depending on the number of layers. TMDs are composed of MX_2, where M is a transition metal and X is a chalcogen. Since various combinations of transition metals and chalcogens are available in the TMD family, interesting characteristics, such as semiconducting, magnetic, or superconducting properties, can be observed depending on M and X. As a result, numerous studies have been extensively conducted on the electrical and optoelectronic applications of 2D-layered TMDs.[1−9] Representative combinations of transition metals and chalcogens for the composition of TMDs are presented in Figure 1a. For example, molybdenum disulfide (MoS_2) is one of the most popular n-type semiconductor TMD materials. Bulk crystal MoS_2 exhibits an indirect bandgap of 1.2 eV, whereas monolayer MoS_2 has a direct bandgap of 1.9 eV and can be utilized as a channel layer in a variety of optoelectronics.[10,11] Moreover, monolayer MoS_2 has been widely investigated in the field of spintronics and valleytronics due to its strong intrinsic magnetic fields that result when inversion symmetry is broken.[12−15] Furthermore, the large-area synthesis of layered TMDs by molecular beam epitaxy or chemical vapor deposition (CVD) allows the realization of more practical TMD-based applications beyond a single device.[16−22]

Interestingly, the electrical and optoelectronic properties of TMDs sensitively depend on the interface environment due to the 2D nature and large surface-to-volume ratio. The interfaces of TMD-based semiconducting devices, for example, field-effect transistors (FETs), can be classified into three types: (1) the interface exists between the TMD and air (generally denoted by the surface), (2) the interface exists between the TMD and the top or bottom dielectric, and (3) the interface exists between the TMD and metal contacts, as denoted in Figure 1b. Additionally, native defects, such as adatoms or vacancies on the surface of TMDs, play a pivotal role in the determination of the material's electrical characteristics. It is well-known that these interfacial properties can significantly

Received: April 2, 2019
Accepted: July 22, 2019
Published: July 22, 2019

Downloaded via 221.167.247.9 on March 8, 2020 at 12:26:20 (UTC).
See https://pubs.acs.org/sharingguidelines for options on how to legitimately share published articles.

© 2019 American Chemical Society

DOI: 10.1021/acsnano.9b02540
ACS Nano 2019, 13, 9713−9734

Figure 1. (a) Representative constituent metal and chalcogen elements of TMDs. (b) A schematic of the typical three-terminal FET structure with three representative interfaces: between (1) the TMD semiconducting layer and (a) the ambient (air or vacuum), (2) the gate dielectric layer, and (3) metal *S*/*D* contacts.

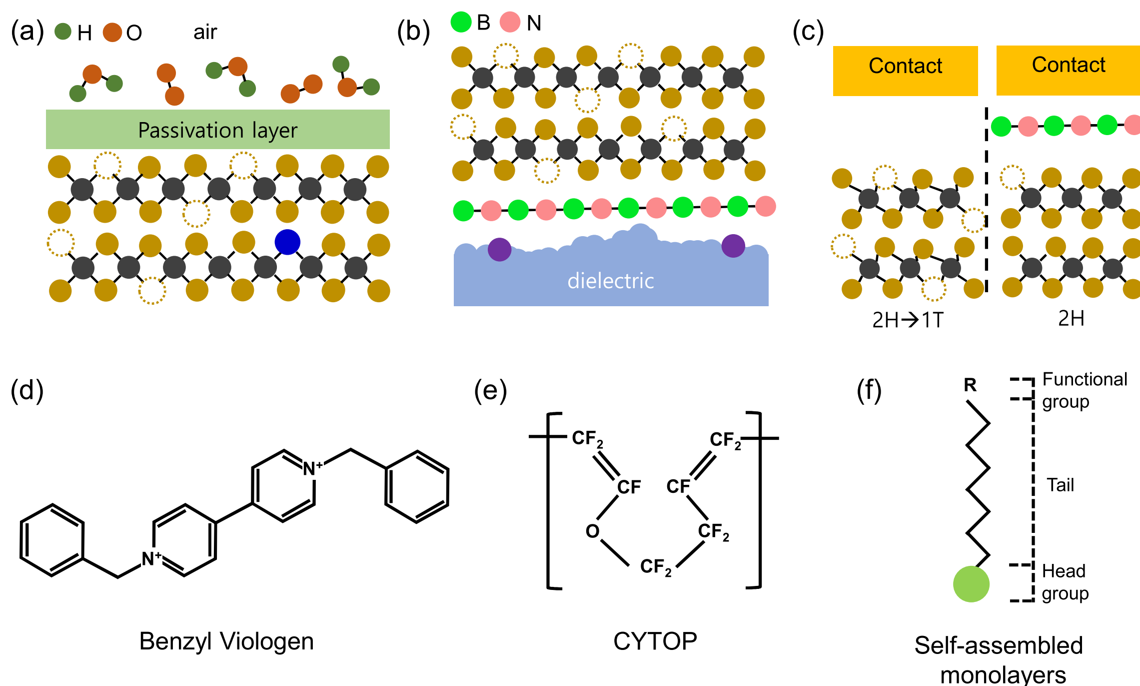

Figure 2. (a−c) Schematic images of interface engineering. (a) The introduction of passivation layers to prevent undesirable adsorption in the ambient, (b) the introduction of an atomically smooth dielectric interlayer to reduce charge scattering, and (c) changing the phase of TMDs from the semiconducting phase (2H) to the metallic phase (1T) or the introduction of a thin insulating layer to suppress Fermi-level pinning effects and reduce contact resistance. (d−f) Schematics of molecular structures of representative organic molecules and polymers: (d) BV, (e) CYTOP, and (f) SAM molecules.

DOI: 10.1021/acsnano.9b02540
ACS Nano 2019, 13, 9713−9734

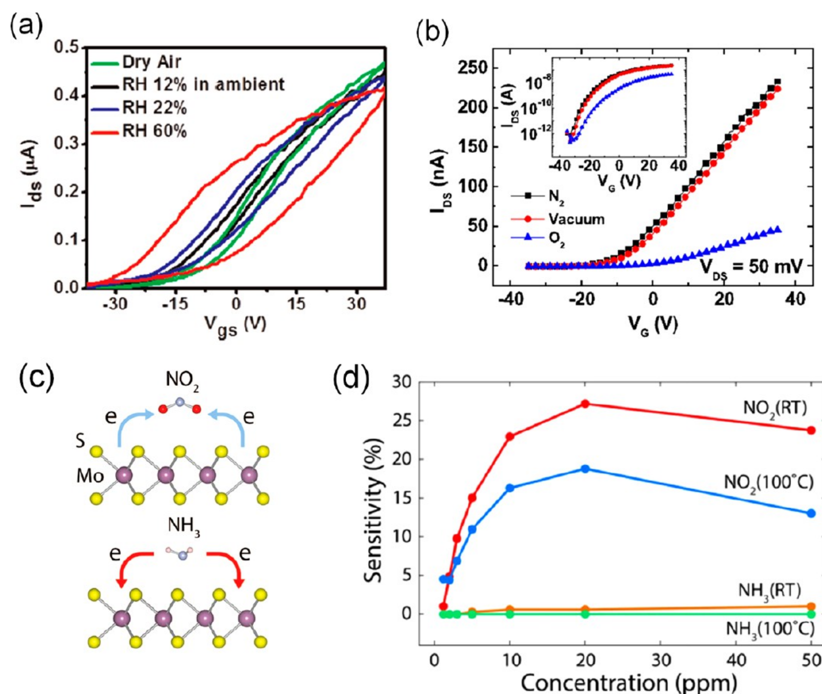

Figure 3. (a) Hysteresis in a single-layer MoS_2 transistor in controlled humidity under the same sweeping rate of gate voltage at 0.5 V/s and V_{DS} = 0.5 V. The humidity increased from 12% RH (black curve) to 22% RH (blue curve) and finally to 60% RH (red curve). Reproduced with permission from ref 23. Copyright 2012 American Chemical Society. (b) I_{DS}−V_{GS} characteristics of a nonpassivated MoS_2 FET in nitrogen, vacuum, and oxygen environments. The inset shows a semilogarithmic plot. Reproduced with permission from ref 24. Copyright 2013 IOP Publishing. (c) Schematics of the charge density differences of MoS_2 in the presence of NO_2 (top) and NH_3 (bottom) gas molecules. NO_2 molecules on the surface of MoS_2 act as electron acceptors, whereas NH_3 molecules act as electron donors. (d) A comparison of the NO_2 and NH_3 sensitivities at different gas concentrations and operating temperatures. The highest selectivity of NO_2 to NH_3 was obtained when the concentration reached 20 ppm at 100 uC. Reproduced with permission from ref 56. Copyright 2015 Springer Nature Publishing.

affect the electrical and optoelectronic characteristics of TMD-based devices, such as the current level, subthreshold swing (*SS*) value, and carrier mobility. For example, adsorbed water molecules or oxygen molecules on the surface of TMDs can capture charge carriers, resulting in the degradation of the source−drain (*S*/*D*) current (I_{SD}) in FET applications.[23,24] In the channel layer, charged impurities, as well as the roughness of the dielectric layer, located between the dielectric layer and the TMD can behave as trap sites or scattering centers.[25−32] In addition, interfacial defects located at the contact regions can degrade carrier injection properties *via* Fermi-level pinning phenomena.[33−35]

Therefore, a promising strategy for realizing further electrically improved TMD-based device applications is efficient interface engineering with the consideration of the interfacial properties, such as interfacial defect or coupling sites, as well as utilizing the intrinsic properties of TMDs, such as metallic (*e.g.*, NbS_2), semi-metallic (*e.g.*, WTe_2), semi-conducting (*e.g.*, MoS_2 and WSe_2), and superconducting (*e.g.*, TaS_2 and $NbSe_2$).[7,36−41] In this manner, there have been many efforts to introduce a surface passivation layer (Figure 2a) or interlayer, for example, hexagonal boron nitride (h-BN), between the TMD and the dielectric layer (Figure 2b),[42] phase engineering[43] and a thin insulating interlayer working as a tunneling layer between the metal contact and the TMD channel (Figure 2c).[44] In particular, organic molecule and polymer treatments conducted directly on TMDs by using simple solution processing, such as immersion, spin-coating, or vapor deposition processing have attracted substantial attention as facile methodologies for modulating the electrical properties of TMD materials. For example, the electron density in TMD channel layers can be significantly increased *via* a simple surface treatment with benzyl viologen (BV) (Figure 2d), which can serve as an n-type surface charge-transfer dopant.[45] Additionally, a low-dielectric constant (low-*k*) polymer (*e.g.*, CYTOP (Figure 2e)) interlayer, located between a high-*k* dielectric layer and a p-type TMD semiconductor, can enhance the electrical properties of TMD-based FETs, including the carrier mobility and *SS* value by preventing unwanted effects from the scattering and dispersion of defects during the atomic layer deposition (ALD) process.[46] Furthermore, a self-assembled monolayer (SAM) can be introduced to not only passivate the surface of the dielectric layer or the structural vacancies of TMDs but also modulate the electrical properties of TMDs from a change in electric dipole moments.[47]

This review highlights recent progress in the interface engineering of TMDs with various organic molecules and polymers to improve or modulate their electrical and optoelectronic characteristics and how they can affect the electrical and optoelectronic characteristics of TMDs-based devices. The key advantage of using organic molecules and polymers is to utilize the various combination of organic materials which have different functionalities. Moreover, these materials can be directly conducted onto the different class of interfaces to modulate interfacial properties *via* relatively facile processing. There are some review articles published related to interface engineering in TMD-based electronics, but their

DOI: 10.1021/acsnano.9b02540
ACS Nano 2019, 13, 9713−9734

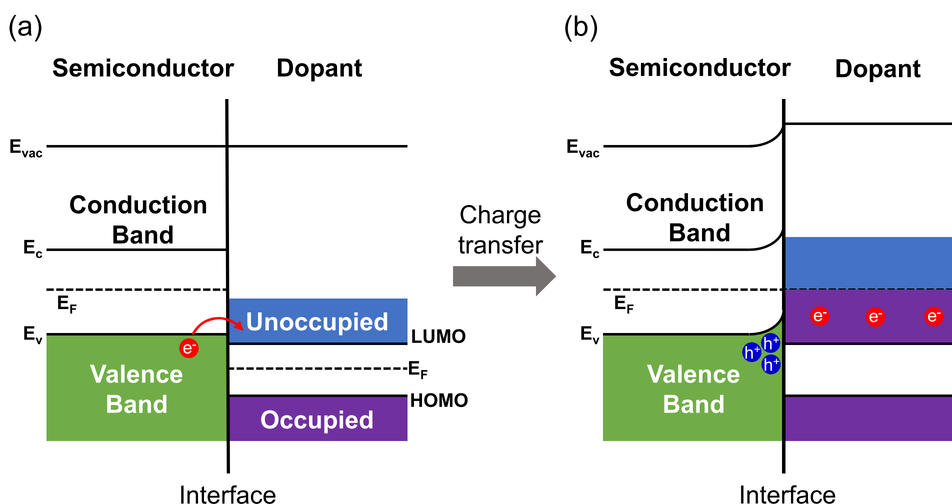

Figure 4. Schematic energy diagrams for the p-type SCTD process (a) before and (b) after charge transfer to the TMD by the organic dopant.

dedications lie on the different point of view. For example, Allain *et al.* dedicated to the physical analysis of the electrical contacts depending on the device structure, the class of TMDs, metal and type of contacts.[2] Schmidt *et al.* specifically focused on the charge transport characteristics of TMDs depending on channel doping.[48] Jariwala *et al.* provided an overview of the characteristics of mixed dimensional heterostructures between 2D vdW materials and other dimensional materials, such as 0D quantum dots, 1D nanowires, and 3D semiconductors,[49] and Bertolazzi *et al.* focused on molecular chemistry for tuning the properties of TMDs.[50] Although several excellent reviews have already introduced the strategies for the interface engineering of TMDs,[48−55] the overarching aim of this review is to provide an overview of the recent achievements in modulating the electrical and optoelectronic characteristics of TMDs *via* organic molecule or polymer treatments. Specifically, we will introduce different engineering strategies depending on whether the interface is with air (or vacuum), the gate dielectric, or S/D contacts by using only organic molecules and polymers that enable tailoring the electrical and optoelectronic characteristics of TMDs with a high degree of design freedom. Therefore, this review article can be beneficial to the readers by reporting the current issues with the interfacial properties of TMDs and the efforts to address them *via* efficient interface engineering. Moreover, it will provide a thorough insight of interface engineering, describing the significance, opportunities, and the challenges of this research field.

Interface Engineering between TMDs and Air. In the typically employed bottom-gated FET structure, the channel layer is inevitably exposed to ambient conditions. In particular, because TMDs exhibit a large surface-to-volume ratio, the electrical and optoelectronic characteristics are significantly affected by the surface-air conditions. For example, the adsorption of oxygen or water molecules onto the MoS_2 channel can affect the electrical characteristics of MoS_2 FETs by capturing electrons due to the large electronegativity of oxygen. In particular, Late *et al.* reported a large hysteresis window of MoS_2 FETs during dual V_{GS} sweeps as the room humidity (RH) increased, resulting in a reduced channel current (Figure 3a).[23] Similar to this result, an oxygen-rich environment can also degrade the electrical performance, including the on/off ratio and carrier mobility.[24] Due to this environmental sensitivity, MoS_2 FETs could be used as chemical sensors based on the surface charge transfer by adsorbed NO_2 or NH_3 (Figure 3c,d).[56] Therefore, introducing functional molecules or polymers to passivate TMDs from air or eliminate natural defects on the surface has been widely investigated to address this issue. In this context, physical encapsulations have been introduced to protect TMDs against adsorption of oxygen or water molecules in air. For example, Kufer *et al.* reported the enhanced electronic and optoelectronic properties such as a high on/off current ratio, narrow hysteresis window, high mobility, high sensitivity, and fast operation in monolayer and bilayer MoS_2 photodetectors by encapsulating them with atomic layer deposited hafnium oxide (HfO_2) that could isolate them from the ambient conditions.[57] However, the processing for the HfO_2 deposition can also create additional sulfur vacancies which may degrade the long-term stability. Lee *et al.* reported highly stable MoS_2 FETs encapsulated by h-BN to improve the environmental stability as well as interfacial properties of the TMD channels,[58] however achieving a well-aligned vdW heterostructure requires low-yield complicated processing that can be a bottleneck to realize further practical applications. Others utilized polymer thin films such as CYTOP, poly(methyl methacrylate) (PMMA), and poly(4-vinylphenol) (PVP) as encapsulation layers that have the attractive advantage of high-yield, low-cost, and facile implementation to deposit from a processing perspective.[24,46,59] On the contrary to physical encapsulations, functionalized organic dopants, which can donate or withdraw charge carriers, facilitate surface charge-transfer doping (SCTD), determining the carrier density. SCTD is a simple non-invasive and reversible strategy achieved without any physical changes of the TMD channel layer, such as lattice distortion. However, it is relatively hard to change intrinsic states of vacancies or adatoms due to the absence of chemical bonding. Therefore, physically adsorbed dopants could be easily removed under harsh environments such as exposure to organic solvents or high temperature, compared to chemically adsorbed dopants. In this manner, although defect passivation *via* chemical bonding exhibits better environmental stability compared to SCTD, the required chemical reaction conditions including overcoming activation energy of the reaction should be met. In addition, undesirable lattice distortion might be

DOI: 10.1021/acsnano.9b02540
ACS Nano 2019, 13, 9713−9734

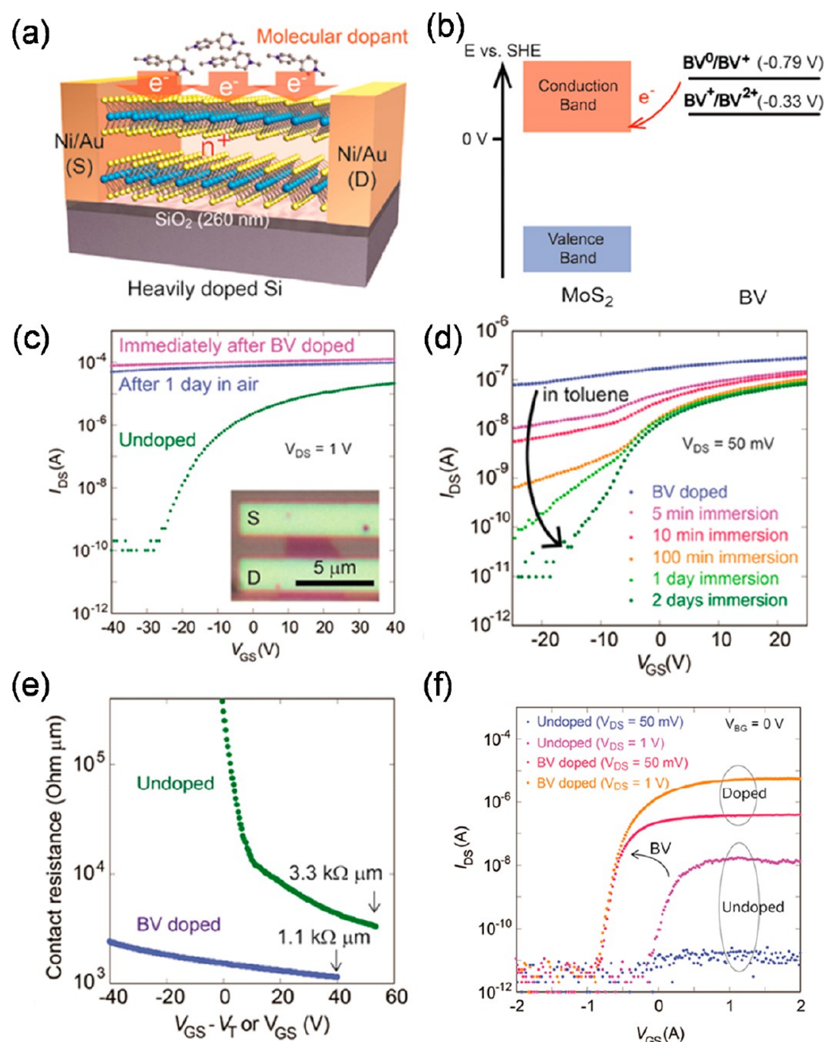

Figure 5. (a) Schematic illustration of a back-gated MoS_2 FET to investigate the effect of SCTD with BV. The phenyl rings are omitted in the schematics of BV molecules for simplification. (b) The energy band diagram of MoS_2 and BV redox states. The conduction band edge of MoS_2 is located at ~0 V *vs* standard hydrogen electrode (SHE), which is lower than the redox potentials of the BV molecules. This energy level offset results in electron donation from BV molecules to MoS_2. (c) Transfer characteristic curves of the device before doping (green), right after BV doping (purple), and after the doped device was kept in air for 1 day (blue) at V_{DS} = 1 V. The inset shows an optical microscope image of the device, consisting of trilayer MoS_2. (d) Transfer characteristics of a BV-doped FET as a function of time of immersion in toluene, depicting the on-demand removal of BV surface charge-transfer dopants. As the BV molecules were dissolved away in toluene, the I_{DS}−V_{GS} curves were converted back to the original characteristic profile. (e) The gate-voltage dependence of the measured contact resistance before (green curve) and after (blue curve) BV doping. (f) Transfer characteristic curves of the top-gate device before (blue and purple) and after (pink and orange) BV treatment at V_{DS} = 50 mV and 1 V. The substrate was grounded during the measurements. Reproduced with permission from ref 45. Copyright 2014 American Chemical Society.

caused by the steric effects from adsorbed molecules, and doping concentration could be self-limited due to the limited number of bonding sites. Also, if the chemically adsorbed molecules have electric dipole moments, additional charge transfer will be feasible, similar to the same process of SCTD. Therefore, depending on the point of view or the circumstances, the advantages can be disadvantages and *vice versa*. Therefore, it is important to choose which method is more appropriate, considering the purpose of the surface treatment. In this section, we will describe the recent progress to engineer the surface properties of TMDs.

One of the important issues in the field of TMDs is the change of the charge concentration or the type of majority carrier that enables them to be utilized for realizing complementary applications. As a response of these demands, SCTD, which is a method of charge transfer between surface dopants and the semiconducting channel, is a widely used approach owing to its simple nondestructive method achieved without any physical damage to the TMD channel layer and is even reversible by attaching and detaching the dopants, as well as substitutional doping and the work function engineering of electrodes. Figure 4 shows the SCTD mechanism with the energy diagram between a TMD channel layer and a p-type organic surface dopant. When a p-type organic dopant, having a larger electron affinity than the underlying semiconductor, is introduced, the energy level of the lowest unoccupied molecular orbital (LUMO) of the surface dopant will be placed below the valence band maximum of the semiconductor. When the surface dopants are attached to the semiconductor layer, electrons will transfer to the surface dopants from the semiconductor, and holes accumulate at the interface of the underlying semiconductor layer until

DOI: 10.1021/acsnano.9b02540
ACS Nano 2019, 13, 9713−9734

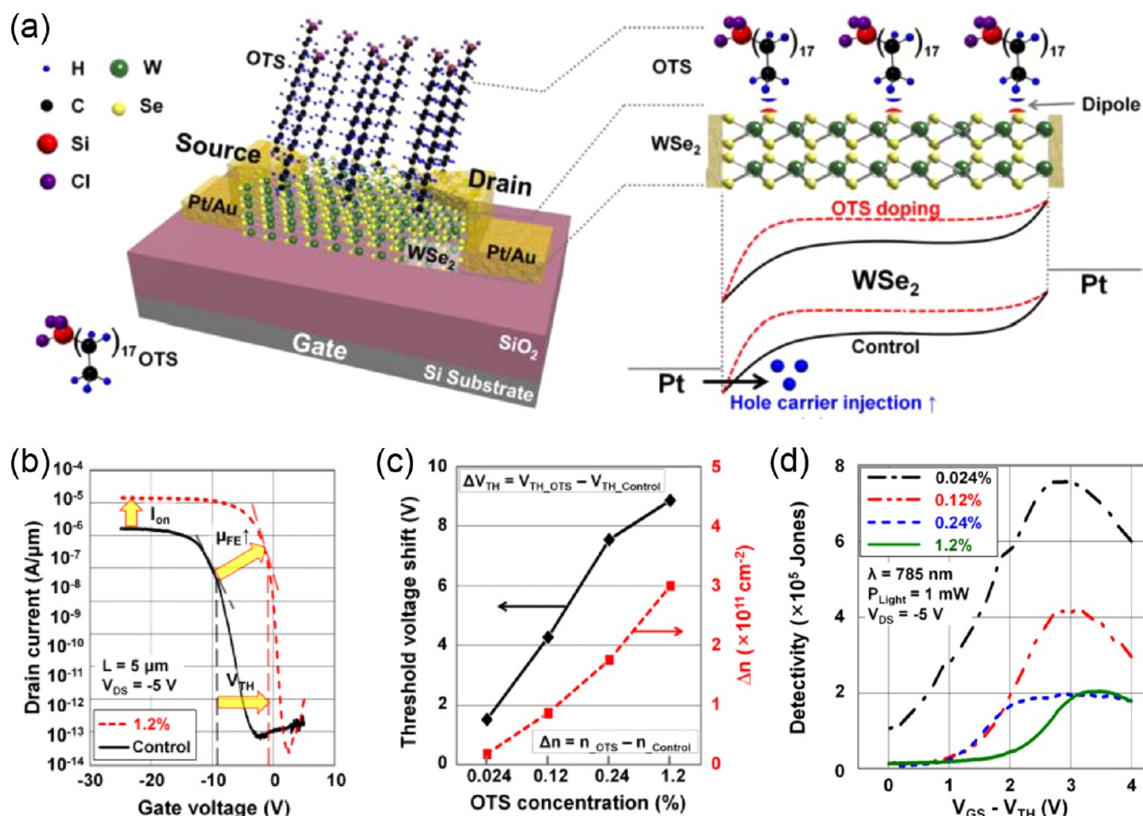

Figure 6. (a) Schematic diagrams of a back-gated transistor fabricated on OTS-doped WSe_2 and the energy band diagrams of Pt−WSe_2−Pt junctions. (b) I_{DS}−V_{GS} transfer curves of (black) undoped and (red) 1.2% OTS-doped WSe_2 FETs (L = 5 μm and V_{DS} = −5 V). (c) The threshold voltage shift ($\Delta V_{TH} = V_{TH\text{-}OTS} - V_{TH\text{-}Control}$) and carrier concentration increase ($\Delta n = n_{OTS} - n_{Control}$) as a function of OTS concentration (0.024%, 0.12%, 0.24%, and 1.2%). (d) Photodetectivity as a function of $V_{GS} - V_{TH}$ (between 0 and 4 V in the off-state) extracted from OTS-doped WSe_2 photodetectors (V_{DS} = −5 V). Reproduced with permission from ref 60. Copyright 2015 American Chemical Society.

equilibrium is reached due to the difference in energy levels. Therefore, the energy band structure of the semiconductor will be bent upward near its surface, resulting in the p-doped semiconductor layer (Figure 4b). Similarly, when a n-type dopant is introduced, electron accumulation at the surface of the semiconductor will result in its energy band structure being bent downward near the semiconductor surface. It should be noted that this behavior is more effective in modulating the electrical or optoelectronic characteristics of 2D TMDs due to their large surface-to-volume ratio. In addition, many research groups have designed a variety of organic molecules having different energy levels (HOMO and LUMO levels) that can be utilized as dopants. The following includes the recently published representative results of SCTD with functionalized organic molecules.

Among the functionalized organic dopants, one of the most popular candidates for SCTD is BV, which has been widely used as an n-type dopant for carbon nanotubes and graphene.[45] Due to the difference between the valence band energy level of MoS_2 and the LUMO level of BV (Figure 5b), a significantly improved electrical performance in doped-MoS_2 FETs, especially in the carrier concentration and contact resistance, was achieved by transferring electrons from BV to MoS_2 (Figure 5c,e). In addition, because the neutral viologen molecule can spontaneously donate electrons to MoS_2 by a redox reaction, BV exhibited good stability as an n-type dopant in ambient air.[45] However, this processing results in a critical disadvantage that the ability of gate modulation was dramatically degraded because of the strong electron-donating behavior of BV. To address this issue, Kiriya *et al.* suggested an immersion process of the doped MoS_2 in toluene to eliminate n-type dopants onto the MoS_2 surface. Depending on the immersion time, the ability of current modulation *via* gating was facilely changed (Figure 5d). Furthermore, significantly smaller contact resistance and improved *SS* values were extracted from the BV-doped MoS_2 FETs, therefore, this strategy enables us to operate MoS_2 FETs with a low-operation voltage (Figure 5e,f).

SCTD can also be employed to change the optoelectronic properties of other TMDs. Kang *et al.* reported that octadecyltrichlorosilane (OTS), which has been widely used as a p-type dopant, could suppress the negative charge carrier density in the p-type WSe_2 channel layer.[60] By controlling the concentration of OTS, the doping level in the WSe_2 channel layer could be controllable from 2.1×10^{11} to $5.2 \times 10^{11}/cm^2$. As a result, substantially improved electrical performances were achieved including 10-times higher I_{DS} with abrupt switching characteristics, good mobility, and high on/off ratio as well as a threshold voltage (V_{TH}) shift in the positive direction due to the increase in the hole concentration (Figure 6c). Furthermore, the ability to modulate the optoelectronic characteristics, such as responsivity and detectivity, of OTS-doped WSe_2 was shown by changing the doping concentration (Figure 6c,d). These doping effects were also revisible *via* additional post-thermal treatments. The intrinsic dipole moment of the OTS molecules could originate the charge-

DOI: 10.1021/acsnano.9b02540
ACS Nano 2019, 13, 9713−9734

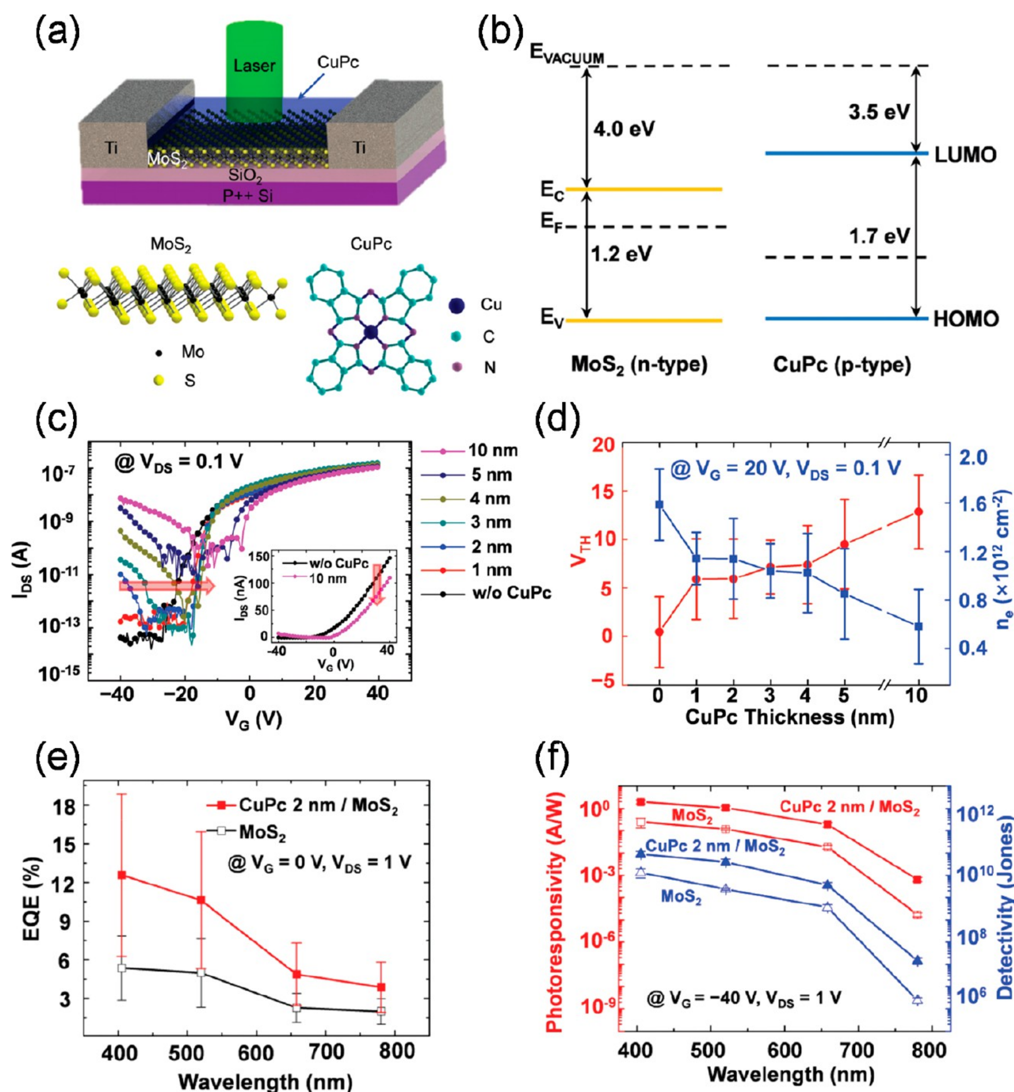

Figure 7. (a) A schematic of a CuPc/MoS_2 device illuminated by a laser. The molecular structures of the MoS_2 and CuPc are also shown. (b) A schematic of the energy band alignment of CuPc/MoS_2 before stacking. (c) I_{DS}−V_{GS} curves on a semilogarithmic scale of the MoS_2 FETs without (labeled with "w/o CuPc") and with a CuPc layer of various thicknesses (1, 2, 3, 4, 5, and 10 nm) measured at fixed V_{DS} = 0.1 V. The inset is a linear plot of the I_{DS}−V_{GS} curves for a pristine MoS_2 FET without a CuPc layer and a 10 nm-thick CuPc/MoS_2 hybrid FET. The arrows indicate shifts in threshold voltages and currents. (d) The threshold voltage and electron carrier concentrations for a pristine MoS_2 FET and CuPc/MoS_2 FETs as a function of the thickness of the CuPc layer. (e) The EQE, (f) photoresponsivity, and detectivity of pristine MoS_2 and CuPc/MoS_2 photodetectors as a function of the wavelength of illumination. Reproduced with permission from ref 62. Copyright 2015 Royal Society of Chemistry.

transfer behavior, providing charges at the surface of WSe_2, as illustrated in Figure 6a.

For the SCTD methodology, vacuum processing has also been extensively used where the doping effects are highly sensitive to the thickness of the organic doping layer. Recently, the phthalocyanine (Pc) molecule family, such as CuPc, CuTsPc, or FeTsPc, have shown attractive advantages as surface charge-transfer dopants.[61] They are physically adsorbed on the surface of TMDs similar to other surface charge-transfer dopants, therefore they will not affect the crystalline lattice of the TMDs as non-invasive molecular dopants. Also, there are over 70 different types of molecules in the Pc compound family, offering opportunities to introduce a wide range of electrical characteristics compared to other conventional molecule dopants such as BV and OTS. In contrast to other organic polymers exhibiting a bulky nature, Pc molecules have a compatible diameter with emerging miniaturized devices. In this context, Pak *et al.* reported the modulation of the optoelectronic properties of MoS_2 phototransistors by depositing copper phthalocyanine (CuPc), a p-type organic semiconductor, onto the n-type MoS_2 channel layer using a thermal evaporator system.[62] Here, vacuum evaporation has also been extensively used for more precise SCTD where the doping effects are highly sensitive to the thickness of the organic doping layer. Figure 7a presents the schematic images and structure of the CuPc-deposited MoS_2 FETs. Due to the energy level difference between CuPc and MoS_2, as illustrated in Figure 7b, the charge transfer simultaneously occurred between CuPc and MoS_2, resulting in the modulation of the carrier concentration in the MoS_2 channel layer. As expected, the threshold voltage of CuPC-doped MoS_2 FETs was shifted in the positive gate voltage direction (Figure 7c). Until the thickness of CuPC increased to 10 nm, the electrical characteristics including the threshold voltage, electron

DOI: 10.1021/acsnano.9b02540
ACS Nano 2019, 13, 9713−9734

Table 1. Summary of Recent Doping Processes in TMDs with Organic Molecules

material	dopant	year	dopant type	method	performance	stability	ref
MoS_2	F4-TCNQ, TCNQ	2013	p-type	drop-casting	increased n_h		63
	CuPc	2015	p-type	thermal evaporation	ΔV_{TH} = 12.4 V	physisorption	62
	FeTsPc	2018	p-type	soak	ΔV_{TH} = 6.00 V	physisorption, unstable	61
	CuTsPc	2018	p-type	soak	ΔV_{TH} = 18.0 V	physisorption, stable	61
	APTMS	2013	n-type	soak (substrate SAM)	$\Delta\mu_e$ = 1.41 $cm^2/V{\cdot}s$	–	64
	PEI	2013	n-type	soak	$\Delta\mu_e$ = 12.3 $cm^2/V{\cdot}s$	unstable	65
	TTF	2013	n-type	soak	increased n_e	–	66
	BV	2014	n-type	soak	degenerate doping	chemisorption, stable	45
	APTMS	2015	n-type	Soak	$\Delta\mu_e$ = 113 $cm^2/V{\cdot}s$	unstable	67
	MEA	2015	n-type	soak	$\Delta n_e = 3.70 \times 10^{12}$ cm^{-2}	chemisorption, stable	47
	$(2\text{-Fc-DMBI})_2$	2015	n-type	soak	$\Delta n_e = 6.30 \times 10^{12}$ cm^{-2}	–	68
	2-Fc-DMBI-H	2015	n-type	soak	$\Delta n_e = 5.20 \times 10^{12}$ cm^{-2}	–	68
	PTSA	2015	n-type	soak	$\Delta\mu_e$ = 61.4 $cm^2/V{\cdot}s$, $\Delta n_e = 2.37 \times 10^{12}$ cm^{-2}	stable	69
	Alq_3 NPs	2017	n-type	drop-casting	increased n_e	–	70
	Na_2TsPc	2018	n-type	soak	ΔV_{TH} = −4 V	physisorption, unstable	61
	PPh_3	2018	n-type	spin-coating	$\Delta\mu_e$ = 229 $cm^2/V{\cdot}s$, $\Delta n_e = 8.19 \times 10^{12}$ cm^{-2}	physisorption, unstable	71
WS_2	F4-TCNQ	2014	p-type	drop-casting	ΔV_{TH} = 50 V	–	72
$MoSe_2$	PDPP3T	2018	n-type	spin-coating	$\Delta\mu_e$ = 72.2 $cm^2/V{\cdot}s$	–	73
WSe_2	OTS	2015	p-type	soak	$\Delta\mu_h$ = 136 $cm^2/V{\cdot}s$	unstable	67
	OTS	2015	p-type	soak	$\Delta\mu_h$ = 162 $cm^2/V{\cdot}s$	unstable	60
	FeTsPc	2018	p-type	soak	ΔV_{TH} = 27.0 V	physisorption, stable	61

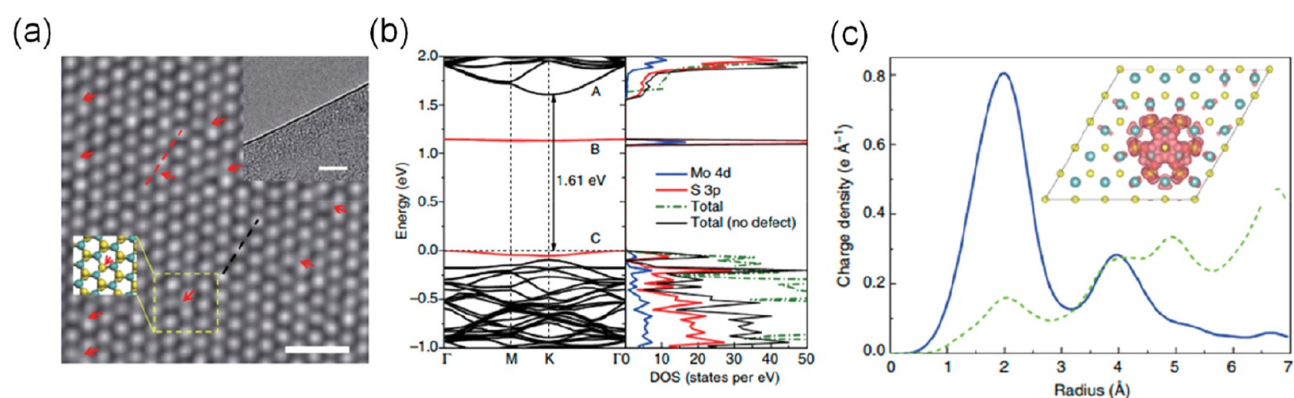

Figure 8. (a) Atomic structure of a single-layer MoS_2 by aberration-corrected TEM. The sulfur vacancies (SVs) are highlighted by red arrows. The upper inset shows the MoS_2 sample edge to confirm the single-layer nature. The lower inset shows a schematic of the highlighted region. Scale bar, 10 nm. (b) The band structure (left) and partial DOS (PDOS, right) for a single-layer MoS_2 5 × 5 supercell with an SV. The localized states are highlighted by red lines. The green dashed line corresponds to the case without SV. (c) Blue solid line corresponds to radial distribution of the charge density for the localized midgap state (B and B) in (b); and green dashed line corresponds to radial distribution of the charge density for the delocalized top of valence band in perfect MoS_2. The origin is located at the SV. The inset is the isosurface of the decomposed charge density corresponding to the band B in (b). Reproduced with permission from ref 76. Copyright 2013 Springer Nature Publishing.

density, and channel current were successfully modulated (Figure 7d). In addition, better optoelectronic performances were exhibited by the CuPC-doped MoS_2 channel layer because the photogenerated electron−hole pairs could be easily separated at the junction between n-type MoS_2 and p-type CuPc due to the energy level difference. Therefore, the external quantum efficiency (EQE), photoresponsivity, and detectivity of the CuPC-doped MoS_2 were improved when CuPC with the optimum thickness was introduced (Figure 7e,f).

The method of SCTD with organic dopants shows a promising possibility to facilely modulate the electrical and optoelectronic characteristics of TMD-based devices. As introduced above, because SCTD is enabled with customized organic molecules using low-temperature processing without any physical damage, many research groups have intensively studied this strategy to achieve desirable device performances. Recent progress in the SCTD of TMDs is summarized in Table 1.[45,47,60−73]

The electrical characteristics of TMDs are also sensitive to the naturally or intentionally created surface defects. For example, sulfur vacancies or adatoms can affect the electrical characteristics such as the carrier concentration and injection properties between the MoS_2 channel layer and the metal contacts in FET applications. Specifically, it has been reported that the sulfur vacancies of MoS_2 could behave as electron-donor sites or hopping sites, leading to a higher I_{DS} from the increased carrier concentration.[74−78] Therefore, we summarize some recent reports on the defect engineering of TMDs by employing organic molecules and polymers and its effects in

DOI: 10.1021/acsnano.9b02540
ACS Nano 2019, 13, 9713−9734

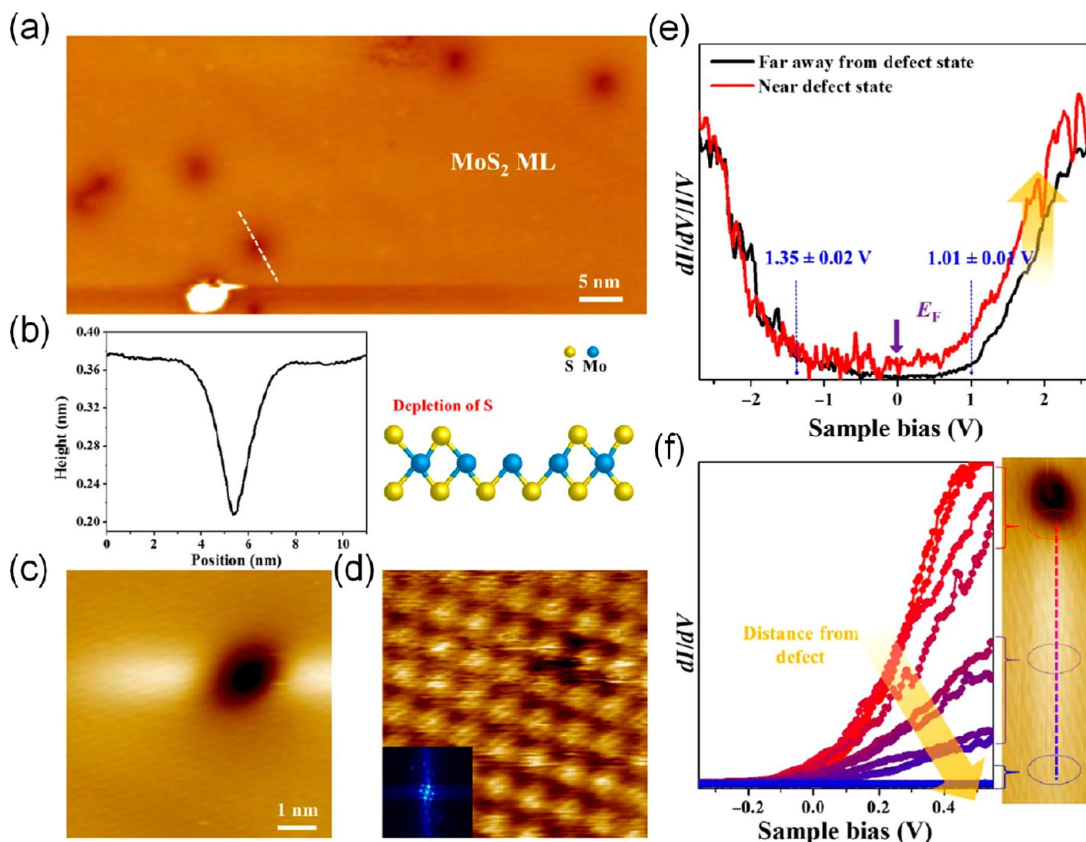

Figure 9. (a) Large-area STM image showing the ML MoS_2 terrace (V_s = 2 V, I_t = 40 pA). (b) The line trace analysis of the white line in (a) and a schematic model of the defects in MoS_2. (c, d) Zoomed-in STM images of a single defect located on the ML MoS_2 in the empty (V_s = 1 V) and filled (V_s = −1 V) states (I_t = 230 pA). Scale bar, 1 nm. (e) STS measured on the terrace of an ML MoS_2; the black spectra are measured far away from the defects, whereas the red spectra are measured near a defect. (f) Spatial STS near the CB edge as a function of the distance from the defect. Reproduced with permission from ref 75. Copyright 2017 American Association for the Advancement of Science.

the electrical and optoelectronic characteristics of TMD-based applications.

Regarding the effect of surface defects on TMDs, Qiu *et al.* reported theoretical analysis that the sulfur vacancies of MoS_2 could behave as electron donors creating energy states in the bandgap of MoS_2.[76] Figure 8a shows scanning tunneling microscope (STM) images showing sulfur vacancies on the surface of defective MoS_2. According to the density functional theory (DFT) calculation, these sulfur vacancies could introduce energy states in the bandgap (Figure 8b), and the electrons in MoS_2 could transport through these states by hopping;[76] therefore, the charge density near the sulfur vacancies could be expected to be larger than that of intrinsic MoS_2 which do not have defects (Figure 8c). Recent experimental evidence supports these theoretical predictions. Park *et al.* directly observed the electron density near the surface defects of CVD-grown monolayer MoS_2 to be higher than that of the surface without defects, especially near sulfur vacancies (as shown in the STM images and cross-sectional profile).[75] The scanning tunneling spectroscopy (STS) image (Figure 9e) shows the local density of states (DOS) at two different positions: The black curve was measured far away from the surface defects, and the red curve was measured near the defect site. Interestingly, an almost metallic state located in the band gap of MoS_2 was observed near the sulfur vacancies due to the highly concentrated electrons. For further investigation, many research groups have tried to intentionally create surface defects on TMDs by using a mild plasma treatment, ion beam irradiation, or electron beam irradiation, and then, organic molecules and polymers have been introduced to passivate the created surface defects.[79,80]

From a material perspective of passivation, the non-oxidizing acid poly(4-styrenesulfonate) (PSS) has been used to eliminate sulfur adatoms or passivate sulfur vacancies on MoS_2.[81] Zhang *et al.* reported that these defects on CVD grown single layer MoS_2 flakes could be successfully passivated by transferring the MoS_2 flakes onto a poly(3,4-ethylenedioxythiophene) poly(4-styrenesulfonate) (PEDOT:PSS) layer, indicating a self-healing MoS_2 *via* the PSS treatment.[81] Figure 10b shows the X-ray photoelectron spectroscopy (XPS) results of intrinsic CVD-grown MoS_2 and self-healed MoS_2 using the PSS treatment. The XPS results for CVD-grown MoS_2 with and without the PSS treatment support that the self-healing process was successfully conducted by revealing a change in the peaks for defective MoS_2 (d-MoS_2) and intrinsic MoS_2 (i-MoS_2). The authors also noted that these results could not be observed when pristine MoS_2 flakes were transferred onto a PEDOT layer without PSS.[81] From the ultraviolet photoelectron spectroscopy (UPS) measurements, the increased work function was observed for self-healed MoS_2; therefore, the difference in energy between the conduction band and Fermi level of self-healed MoS_2 was larger than that of pristine MoS_2, which indicates that the concentration of electrons decreased, resulting in a V_{TH} shift in the positive gate voltage direction and reduced I_{DS} in FET applications (Figure 10d,e). These results are evidence that the sulfur vacancies on MoS_2 work as

DOI: 10.1021/acsnano.9b02540
ACS Nano 2019, 13, 9713−9734

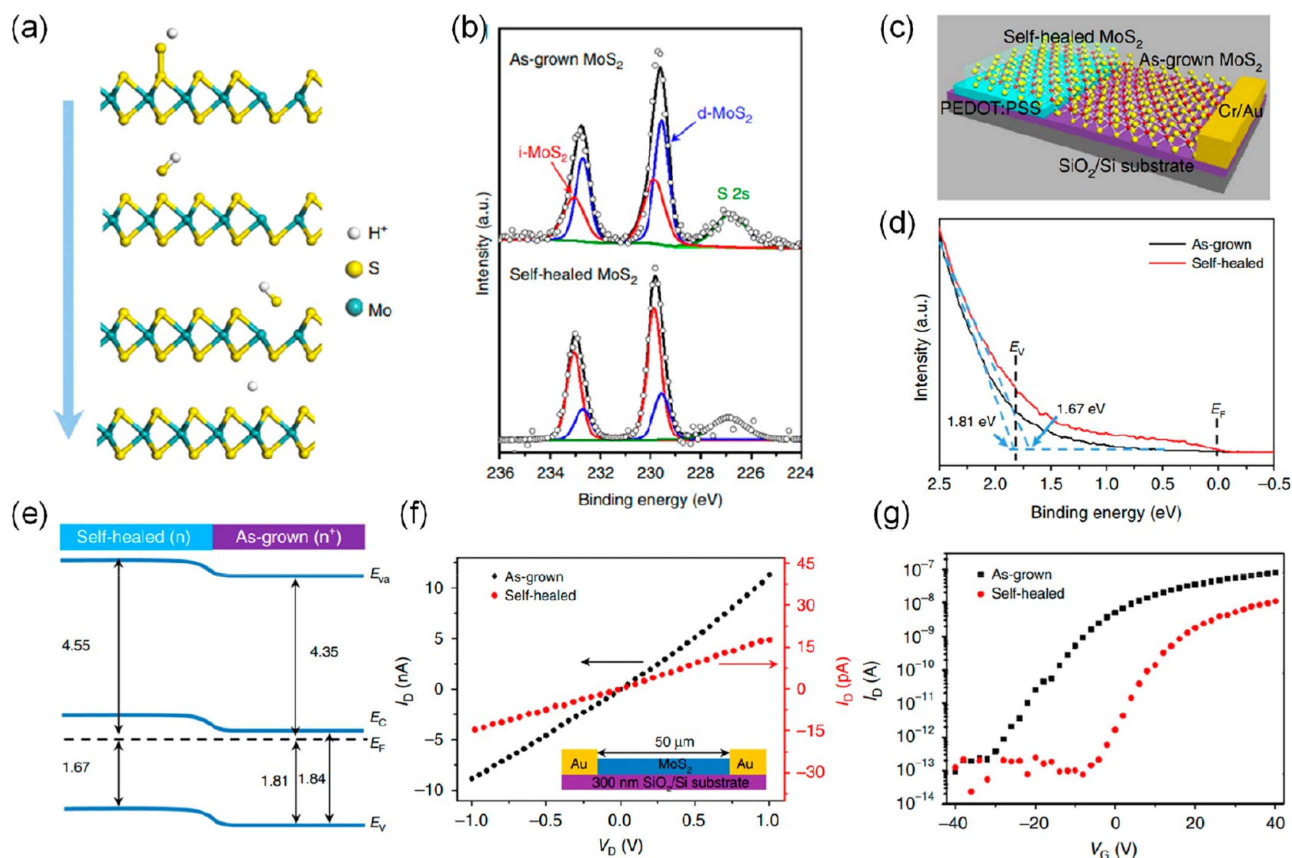

Figure 10. (a) Change in the 2D chemical structure showing the PSS-induced sulfur vacancy self-healing (SVSH) effect. (b) High-resolution XPS of Mo 3d before (top) and after (bottom) the PSS treatment of MoS_2. Red and blue lines represent the intrinsic MoS_2 (i-MoS_2) and defective MoS_2 (d-MoS_2), respectively. (c) A schematic image of the monolayer MoS_2 homojunction. (d) The valence-band spectra from the UPS measurements of as-grown and self-healed monolayer MoS_2. (e) The band diagram of the monolayer MoS_2 homojunction obtained from UPS measurements. (f) Output characteristics and (g) transfer characteristics of a monolayer MoS_2 transistor both before and after PSS-induced SVSH. Reproduced with permission from 81. Copyright 2017 Nature Publishing.

electron-donor states within the bandgap of MoS_2 as well as defect sites. Therefore, through the PSS treatment on the MoS_2 surface, called the self-healing process, the electrical and optoelectronic characteristics could be changed with controlling the density of surface defects.

Thiol-group-containing molecules can also be introduced to passivate the surface defects on MoS_2. Thiols and silanes are well-known materials for the formation of SAMs on the surface of metals and oxide layers, such as Au, Ag, Al_2O_3, and SiO_2.[82−86] The key strength of the thiol molecule is that the functional alkyl group or end group provides a variety of functionality depending on the design of the molecule. Similar to PSS, the sulfur-containing group in thiol molecules could passivate sulfur vacancies or eliminate sulfur adatoms on MoS_2.[47,74,80,87−95] Cho *et al.* investigated the effects on the electrical characteristics of MoS_2 FETs *via* surface engineering with thiol molecules.[89] After introducing thiol molecules onto the MoS_2 surface using a conventional immersion method as shown in Figure 11a, I_{DS} was reduced and accompanied by the simultaneous threshold voltage shift to the positive gate voltage direction that was similar to the results from the self-healing treatment with PSS (Figure 11b,c). However, the *SS* value, primarily determined by the interfacial trap density, was not considerably changed (Figure 11d). These results indicate the adsorbed thiol molecules can decrease the carrier concentration in the MoS_2 channel by passivating the sulfur vacancies that might work as electron-donor sites but not as additional trap sites. Furthermore, this approach provides insights into controlling the electrical properties of MoS_2 by introducing functional molecules that can be coupled with the sulfur vacancies on the MoS_2 surface. This efficient method can also transfer charges from surface dopants to MoS_2 when the adsorbed functional molecules possess their own electric dipole moment. Sim *et al.* reported that mercaptoethylamine (MEA) and 1*H*,1*H*,2*H*,2*H*-perfluorodecanethiol (FDT or PFDT) could be used as surface charge-transfer dopants due to their electric dipole moments as well as passivators of the MoS_2 defect sites.[47] NH_2-containing MEA molecules can donate electrons to MoS_2 because MEA molecules contain lone-pair electrons, while F-containing FDT molecules can withdraw electrons from MoS_2 due to the high electronegativity value of F; therefore, the two modifications can result in the increase and decrease in I_{DS} (Figure 12d,f). For a further accurate investigation, an additional annealing process was conducted afterward to eliminate the adsorbed H_2O and O_2 molecules that can trap the electrons in the MoS_2 channel layer. After the annealing process, I_{DS} increased in MoS_2 layers treated with MEA or FDT due to the detrapping of electrons from adsorbed H_2O and O_2 molecules.

In addition to these experimental results of defect repair in TMDs, the reaction mechanism has also been theoretically studied. From DFT-PBE (Perdew−Burke−Ernzerhof) calculations, Förster *et al.* reported the procedure of the reaction between the thiol-group-containing molecules and MoS_2.[74]

DOI: 10.1021/acsnano.9b02540
ACS Nano 2019, 13, 9713−9734

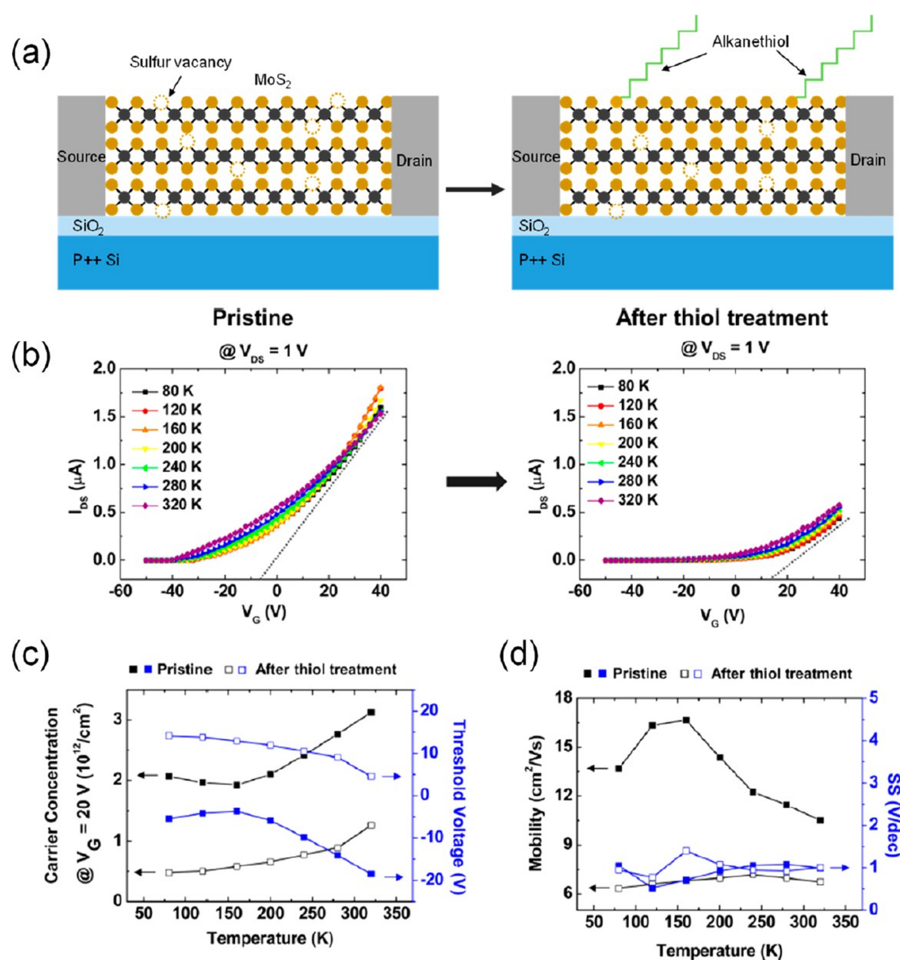

Figure 11. (a) Schematic images of a MoS_2 FET before (left) and after (right) the alkanethiol molecule treatment. (b) I_{DS}–V_{GS} curves measured before and after hexadecanethiol treatment at varying temperatures from 80 to 320 K. (c) The carrier concentration and threshold voltage of a MoS_2 FET as a function of temperature acquired before and after the hexadecanethiol treatment. (d) The mobility and *SS* values of a MoS_2 FET as a function of temperature extracted before and after the hexadecanethiol treatment. Reproduced with permission from ref 88. Copyright 2015 American Chemical Society.

Each of the following chemical reactions between thiol molecules (R–SH) and a defective MoS_2 monolayer, including sulfur monovacancies (V) or sulfur adatoms (A), were reported with experimental evidence.[87,91,93,95,96] The authors also reported the calculated results of the DOS and energy levels of the reaction byproducts using *ab initio* DFT-PBE (Figure 13).

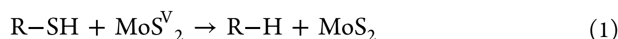

$$\text{R–SH} + \text{MoS}^{V}{}_{2} \rightarrow \text{R–H} + \text{MoS}_{2} \quad (1)$$

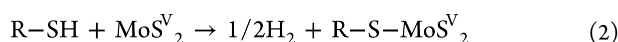

$$\text{R–SH} + \text{MoS}^{V}{}_{2} \rightarrow 1/2\text{H}_{2} + \text{R–S–MoS}^{V}{}_{2} \quad (2)$$

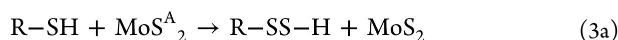

$$\text{R–SH} + \text{MoS}^{A}{}_{2} \rightarrow \text{R–SS–H} + \text{MoS}_{2} \quad (3a)$$

$$\text{R–SS–H} + \text{MoS}^{V}{}_{2} \rightarrow \text{R–SH} + \text{MoS}_{2} \quad (3b)$$

where R, V, and A are alkyl chain, sulfur monovacancies, and sulfur adatoms, respectively. According to the calculations, the surface treatment with thiol molecules could also passivate the surface defects with a low activation energy. This report strongly supports that the strategies using organic functional molecules are highly efficient for tailoring the electrical or optoelectronic characteristics, especially the carrier concentration, in TMD-based applications.

Interface Engineering between TMDs and Dielectrics. When TMDs are used as a semiconducting channel layer in FET applications, the interfacial properties with the gate dielectric and contacts are also important to determine the electrical characteristics. In particular, the defects on the interface between TMDs and the gate dielectric layer can play a key role as trap sites, resulting in a reduced channel current and the poor reliability of TMD FETs.[23,24,32,97−102] Therefore, for better electrical and optoelectronic characteristics, many strategies to improve the quality of interfaces have been reported. For example, inserting h-BN has attracted attention for preventing undesirable effects from charge trapping sites on the oxide layer such as impurity atoms, potassium or sodium, and natural defects.[51−53] However, the realization of the high-quality heterostructure with h-BN and TMDs still requires high-cost, time-consuming, and low-yield processing, so this approach is not suitable to be utilized in practical applications beyond laboratory-scale application. To address this issue, one of the promising approaches is the introduction of functional molecules that can be chemically coupled to the gate dielectric and contacts. Organic molecules can not only eliminate the defects located between the dielectric layer and TMDs but also lower the contact barriers, resulting in better carrier injection properties.[89] Among the representative organic material

DOI: 10.1021/acsnano.9b02540
ACS Nano 2019, 13, 9713–9734

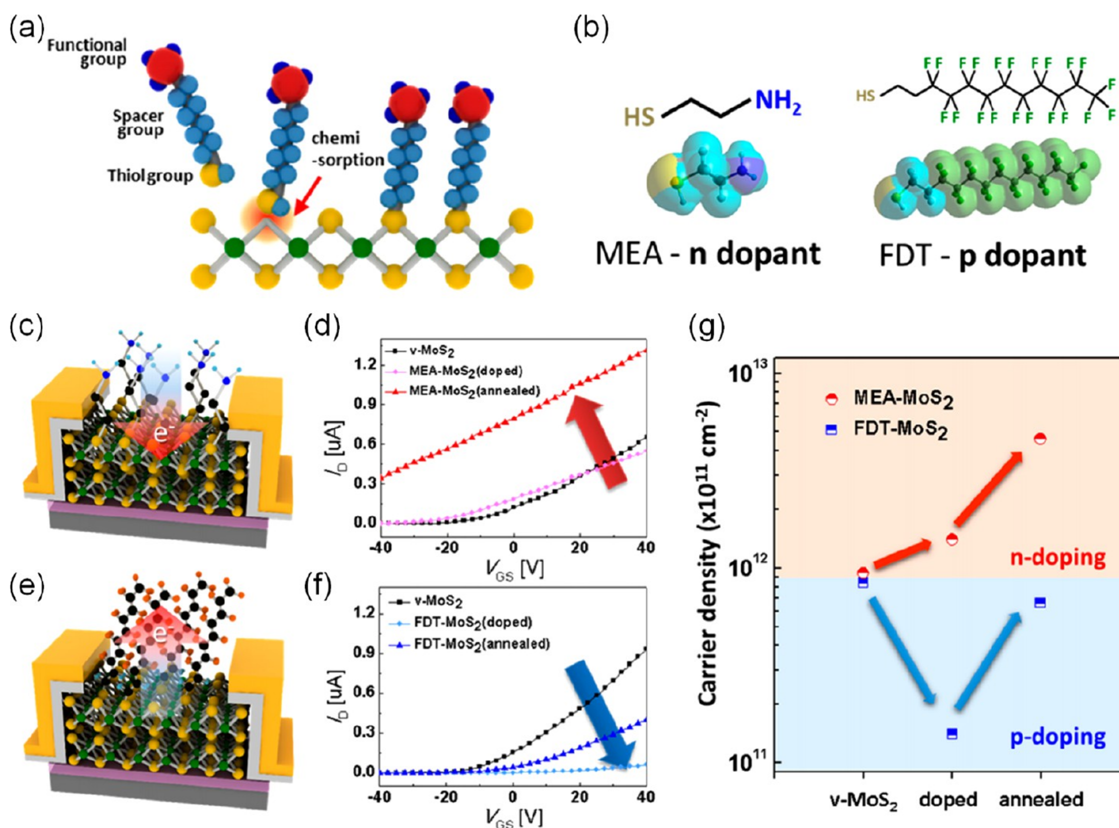

Figure 12. (a) Schematic illustration of the chemisorption of thiol molecules onto sulfur vacancies. (b) Molecular structures of two thiol-terminated molecules containing NH_2 (left, MEA) and a fluorocarbon group (right, FDT) used for the molecular functionalization of v-MoS_2. (c, e) Schematic illustrations presenting the charge-transfer doping of a back-gated MoS_2 FET with MEA and FDT molecules. (d, f) Transfer characteristics of MEA-MoS_2 and FDT-MoS_2 obtained with V_{DS} = 0.5 V; before doping (black line), after doping (blue line), and after doping and annealing (red line). (g) Changes in the carrier density before and after the doping process (measured at V_{GS} = 0 V). Reproduced with permission from ref 47. Copyright 2015 American Chemical Society.

candidates, SAMs widely investigated to eliminate interfacial defects are a representative example of interface engineering using organic material. Typically, molecules of SAM consist of three parts: linker group located at the bottom, backbone located at the middle, and end group located at the top. It has been reported that roughly four factors of SAM interlayer can affect the electrical and optoelectronic characteristics of TMDs, including charge transfer, built-in molecular polarities, modified substrate defect properties, and interfacial property.[52] Therefore, numerous combinations that provide a variety of functionalities depending on the target applications are available. End-functionalized PS directly coupled with hydroxyl groups on underlying oxide layers can deliver efficiently hydrophobic surfaces and eliminate charge trapping sites from hydroxyl groups. However, it cannot allow much molecule design of freedom as well as perfectly aligned monolayers compared to SAM. Although CYTOP is also extensively utilized for introducing an interlayer or encapsulation *via* simple solution processing, relatively thick- and low-*k* interlayer reduces the unit capacitance of the gate dielectric which directly affects IDS. Moreover, the difficulty of the surface energy engineering does not allow the surface modification with functional molecules. In this section, we will introduce the recent efforts to improve interfacial properties by employing functionalized molecules between the TMD channel and dielectric.

To implement more reliable FETs, optimized device structures, as well as physical or chemical engineering at the interface of the TMD channel, have been reported to prevent degradation of the electrical characteristics during operation. Radisavljevic *et al.* reported that further reliable electrical characteristics of MoS_2 FETs could be exhibited by employing a dual-gated structure, even at low-temperature because of reduced phonon scattering, Coulomb scattering, and charged impurities, as shown in Figure 14b.[103] In addition, the gate dielectric layer can also affect the electrical characteristics of MoS_2 FETs. Yu *et al.* reported that the dielectric constant, which is an important parameter of the screening effect of the dielectric layer, determined the effective size of the charged impurities.[104] Because a high-*k* dielectric layer can reduce the effective size of the charged impurities, metal-oxide dielectrics, such as HfO_2 and Al_2O_3, have been widely used in MoS_2 FET applications. Cui *et al.* reported consistent results in WS_2 FETs that the enhanced carrier mobility could be observed when a high-*k* dielectric was introduced, and the theoretical expectation that accounted for effects from intrinsic scattering, surface optical phonon scatterings, and charged impurities also explained the effect of the dielectric constant (Figure 14c,d).[105]

In a perspective of interface properties, many efforts to eliminate interfacial traps and scattering sites have been reported. One of the most efficient approaches has been introducing end-functionalized polymers between the dielectric and the TMD channel layer. Jeong *et al.* reported that dimethylchlorosilane-terminated polystyrene (PS) could be chemically coupled with hydroxyl groups (−OH) that work as interfacial traps on oxide-based gate dielectric layers, such as

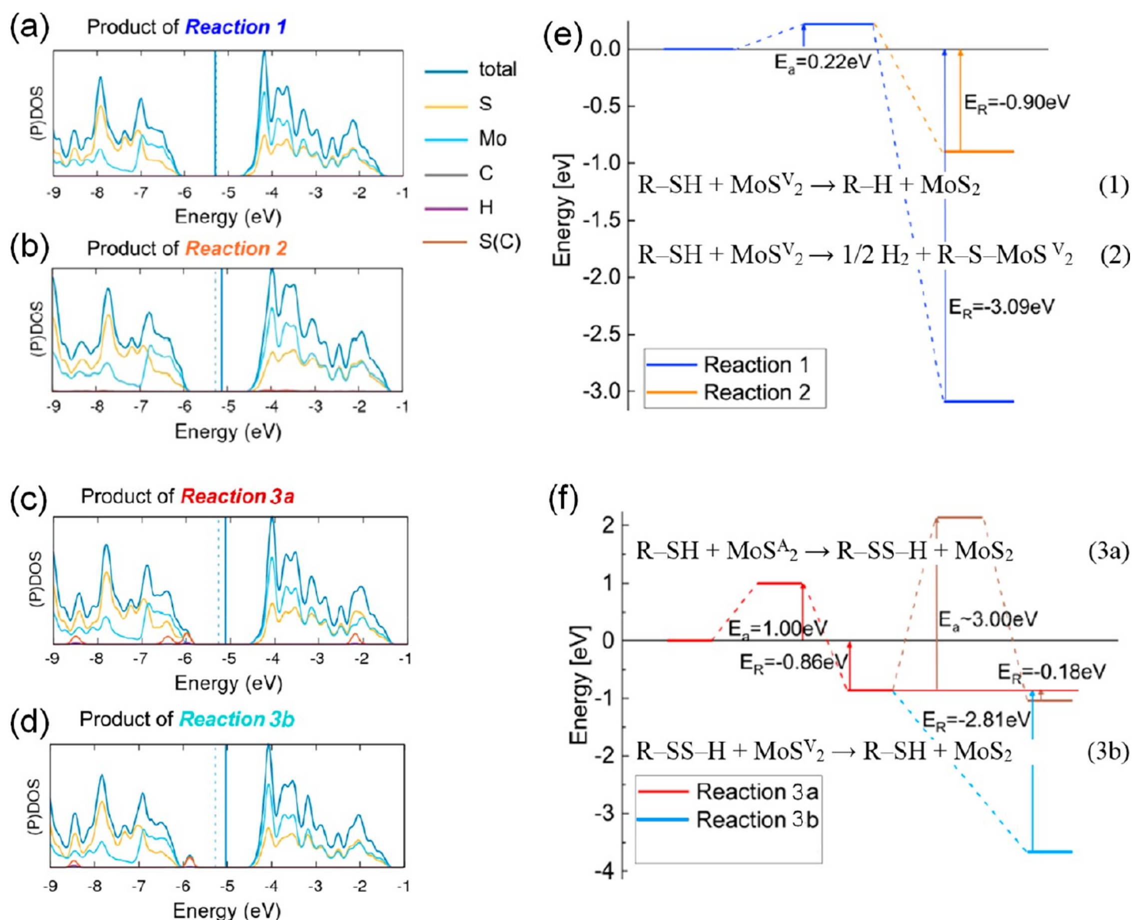

Figure 13. Electronic structures of the products of the vacancy healing process. The total DOS and PDOS of the products of (a) reaction 1 and (b) reaction 2. The electronic structures of the products of the adatom healing process. The total DOS and PDOS of (c) the product of reaction 3a and (d) the product of reaction 3b. All DOS and PDOS functions were convoluted by a Gaussian with a full-width at half-maximum of 0.1 eV. The position of the Fermi level is shown by solid blue lines in defective lattices and by dotted blue lines in the corresponding pristine lattices. (e) The reaction scheme for the sulfur vacancy healing process. E_R denotes the reaction energy, and E_a denotes the activation barrier. The same initial state can lead to two different final states *via* the same transition state. The favorable reaction 1, shown in dark blue, leads to a free CH_4 molecule. The energetics of reaction 2 is displayed in light orange. (f) The reaction scheme of the adatom healing process that starts with reaction 3a and leads to disulfide formation in the presence of extra sulfur atoms on MoS_2, shown in dark red. The alternative subsequent vacancy repair reaction 3b is shown in light blue. Reproduced with permission from ref 74. Copyright 2017 American Chemical Society.

SiO_2 or Al_2O_3.[106] Therefore, improved electrical performances were achieved in the interface-engineered MoS_2 and $MoSe_2$ FETs with ultrathin (~8.6 nm) and uniformly deposited chlorosilane-terminated PS (Figure 15a). Additionally, charged impurities and optical phonons could be eliminated by passivating hydroxyl groups that resulted in significantly increased the carrier mobility thereby suppressing the hysteresis window, as shown in Figure 15b. Note that this strategy has been widely reported to introduce well-crystalline semiconductors in organic FETs, resulting in a substantially improved electrical performance and reliability.[107,108] Organosilanes (−SH_3) can also be an interface engineering material to reduce the density of surface defects or to introduce the functionalized dielectric surfaces (Figure 15c,d). Najmaei *et al.* reported that by introducing a SAM formed with an organosilane on the SiO_2 gate dielectric, better electrical characteristics of TMD-based FETs could be achieved.[109] Because organosilanes can be designed with a variety of combinations, different functionalities, such as different surface energy or electric dipole moments, could be delivered to the surface that resulted in the facile modulation of the electrical characteristics, as shown in Figure 15e,f.[109]

The introduction of thin low-*k* fluoropolymer layers is also an efficient approach to eliminate interfacial defects. Shokouh *et al.* reported that CYTOP can be used to insert a protection buffer layer between the top Al_2O_3 dielectric layer and the WSe_2 channel layer for preventing channel charging (Figure 16a).[46] It is well-known that hydrogen diffusion from an Al_2O_3 dielectric to the underlying channel layer which can degrade the p-type behavior occurs during the Al_2O_3 formation using atomic layer deposition (ALD) in the top-gate structure. Furthermore, because the effect of surface optical phonon scattering could be enhanced when only the high-*k* dielectric was introduced, Shokouh *et al.* claimed that such scatterings could be suppressed by inserting the low-*k* CYTOP dielectric layer between the high-*k* dielectric and TMDs.[46] As shown in Figure 16b−e, the WSe_2 FETs with the CYTOP interlayer on the Al_2O_3 dielectric not only showed a better electrical performance, especially the *SS* value, on/off ratio (Figure 16b,d), and hole mobility (Figure 16c and 16e), but also

DOI: 10.1021/acsnano.9b02540
ACS Nano 2019, 13, 9713−9734

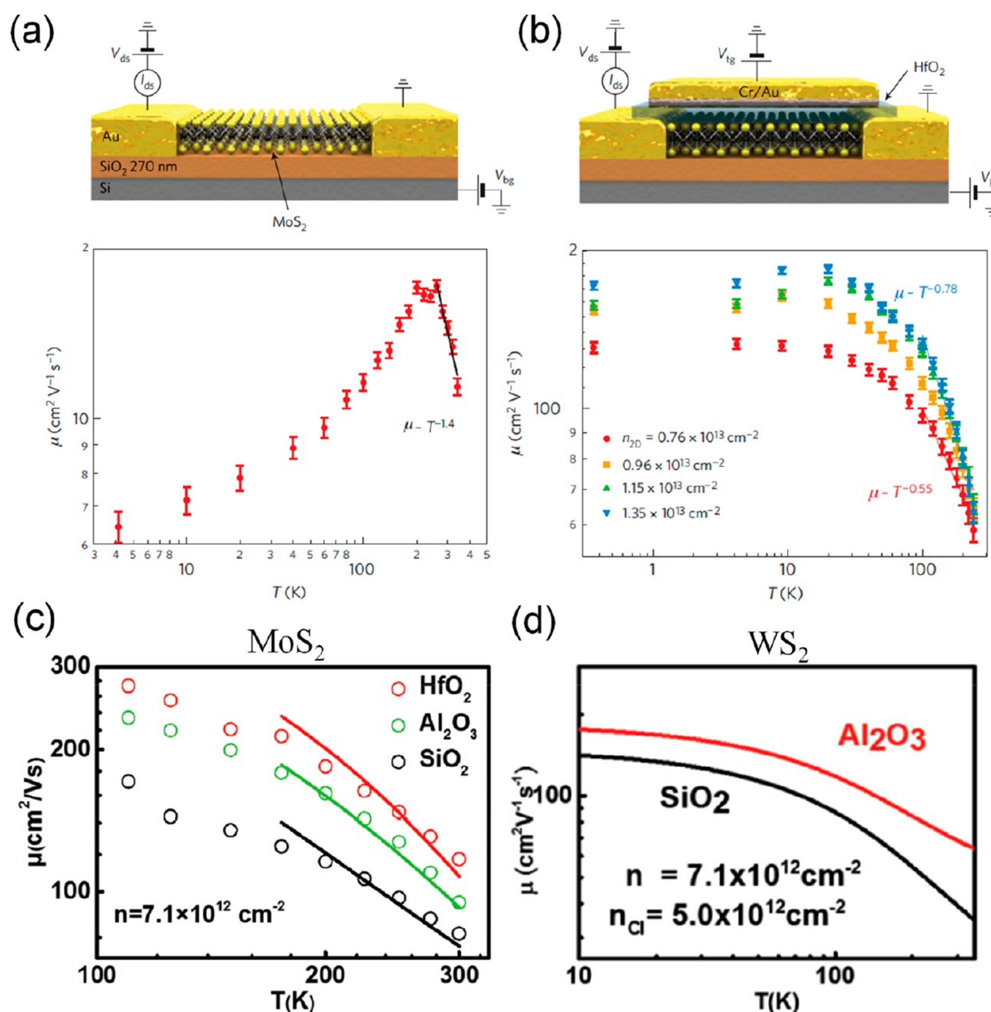

Figure 14. (a) Cross-sectional views of a single-layer MoS_2 FET in a single-gate configuration. (top panel) The dependence of μ on T shows a pronounced low-temperature regime consistent with transport dominated by scattering from charged impurities. Above ~200 K, μ is limited by phonon scattering and follows a $\mu \sim T^{-1.4}$ dependence. (b) Cross-sectional views of a single-layer MoS_2 FET in a dual-gate configuration. (top panel) μ is practically independent of T under 30 K, indicating the screening of charged impurities due to the deposition of the top-gate dielectric. Above ~100 K, μ decreases owing to phonon scattering and follows a $T^{-\gamma}$ dependence with γ = 0.55−0.78. The strongly reduced value of the exponent γ with respect to the single-gated FET (γ = 1.4) is indicative of phonon mode quenching. Reproduced with permission from ref 103. Copyright 2013 Springer Nature Publishing. (c) Field-effect mobility as a function of temperature for three MoS_2 FETs on SiO_2 (black), Al_2O_3 (green), and HfO_2 (red) under $n = 7.1 \times 10^{12}$ cm^{-2} (symbols). Solid lines are the modeling results at high temperature. Reproduced with permission from ref 104. Copyright 2016 John Wiley & Sons, Inc. (d) Theoretical charged impurities (CI)-limited mobility as a function of temperature for monolayer WS_2 on SiO_2 and Al_2O_3 at $n = 7.1 \times 10^{12}$ cm^{-2} and $n_{CI} = 5.0 \times 10^{12}$ cm^{-2}. Reproduced with permission from ref 105. Copyright 2015 John Wiley & Sons, Inc.

contributed to improve the device stability by passivating the WSe_2 surface.

Interface Engineering between TMDs and *S/D* Contacts. Interfacial properties, such as defects and energy barriers, between the *S/D* contacts and a TMD channel also dominantly determine the charge injection in FET applications.[2,34,110,111] In particular, the contact resistance also causes permanent failure *via* thermal stress at the contact region by Joule heating.[112] Therefore, many studies have been reported to reduce the contact resistance by using various contact engineering strategies such as employing a low-work-function metal, phase engineering, laser annealing, a vdW heterostructure. or 1D contacts with ultrathin graphene electrodes.[43,44,110,113−120] However, it remains a challenge to achieve ohmic contact due to a vdW gap between the metal electrodes and the TMD channel layer and interfacial states that can cause Fermi-level pinning, as shown in Figure 17.[111] Therefore, the lowering of the Schottky barrier height or changing the dominant mechanism of carrier injection is highly desirable to realize high-performance TMD-based FET applications with low operation voltages. Generally, considering the relationship between the work function and the energy level of a semiconductor, the Schottky barrier height can be changed by using optimized metal electrodes. However, as mentioned, due to the Fermi-level pinning by interfacial states, the Schottky−Mott rule is not vigorously followed. For example, a huge tunneling current through defects was observed in a three-dimensional (3D) tunneling current mapping image of MoS_2 (Figure 18).[33] In addition, these metal-like defects of MoS_2 contributed to Fermi-level pinning.[121] The extracted Schottky barrier height between MoS_2 and the metal tip of the STM slightly depended on the work function of the metal tip, which indicates that MoS_2 barely follows the Schottky−Mott rule, as shown in Figure 18c.[121] The pinning factor (denoted as

DOI: 10.1021/acsnano.9b02540
ACS Nano 2019, 13, 9713−9734

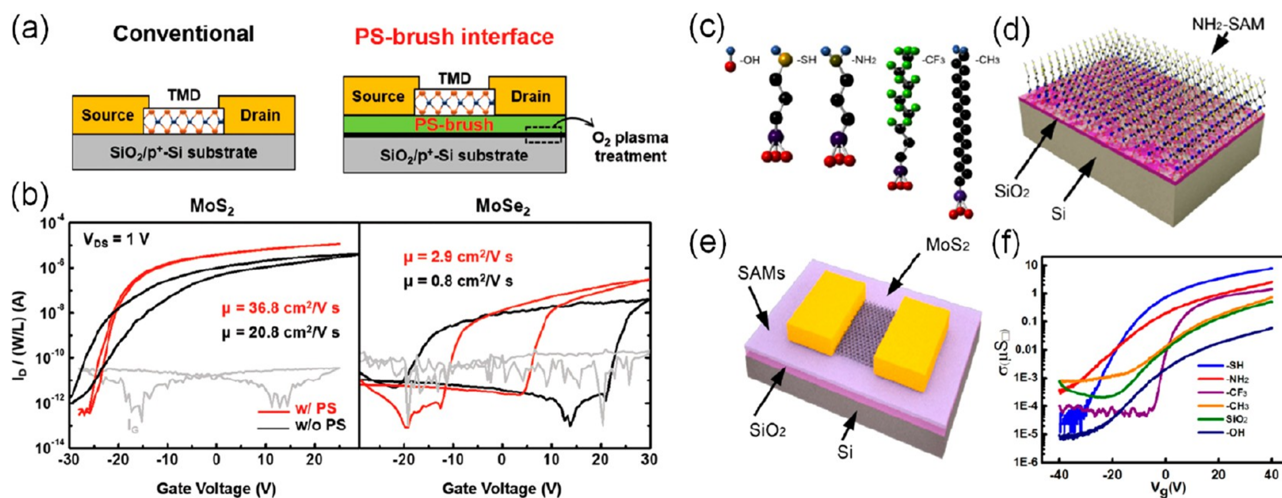

Figure 15. (a) Cross-section schemes illustrating the conventional TMD FET structure and the structure employing a PS-brush layer. The thick black line indicates the O_2 plasma-cleaned SiO_2 surface before introducing a PS-brush layer. (b) $I_{DS}-V_{GS}$ curves of conventional (black line) and PS-brushed (red line) TMD transistors for two representative TMD nanosheets: n-MoS_2 and n-$MoSe_2$. The reduced hysteresis and higher mobility for the PS-brush treated FETs are noted. Reproduced with permission from ref 106. Copyright 2018 John Wiley & Sons, Inc. (c) The ball-and stick-models for SAMs used in the surface functionalization and their orientation relative to MoS_2 monolayers. (d) The assembled configuration of NH_2−SAM molecules as an example of surface functionalization. (e) The schematic of the device configurations in our experiments. (f) Transfer curves of representative measurements on a variety of modified and pristine substrates showing the ON-current modulation through interface engineering. Reproduced with permission from ref 109. Copyright 2014 American Chemical Society.

"S" in Figure 18c) is the slope of the Schottky barrier height *versus* the work function of the metal tip. The pinning factor of the intrinsic MoS_2 surface was determined to be ∼0.3, which is larger than that of the defective MoS_2 surface (∼0.1), indicating that the surface defects of MoS_2 cause Fermi-level pinning and influence the charge injection properties of MoS_2 FETs.

In this manner, many approaches have been proposed to achieve better charge injection properties with organic molecules. As a representative example, the aforementioned SCTD methods have also been employed to reduce the contact resistance of TMD-based FETs. Du *et al.* reported that chemical doping using organic molecules could reduce the contact resistance of multilayer MoS_2 FETs.[65] The MoS_2 doped with polyethylenimine (PEI), an amine-rich aliphatic polymer, exhibited a reduced sheet resistance due to the strong electron-donating behavior of PEI. Similarly, Kiriya *et al.* also drastically reduced the contact resistance values of MoS_2 FETs by employing BV, a strong n-type dopant (Figure 5e),[45] however, these approaches left undesirable phenomena, such as a poor on/off ratio. Therefore, more efficient methods have been suggested to achieve better carrier injection properties, for example, phase engineering to form a metallic phase of the TMD, annealing the contact region to eliminate interfacial defects, or inserting a thin tunneling layer to suppress the Fermi-level pinning phenomenon. If there are a lot of trap states located at the interface between the metal contacts and TMD channels, the Fermi level is pinned and Schottky barrier is formed regardless of metals having different work function. Therefore, it is difficult to achieve ohmic contact because of the Fermi-level pinning effect. In this manner, eliminating interfacial states is considered as a promising method for better charge injection with various contact engineering strategies. It has been theoretically predicted that the insertion of thin layers can reduce the interaction between the metal contacts and the TMD channel and remove the interfacial states that can be the origin of Fermi-level pinning.[122,123] Additionally, Cui *et al.* reported that an inserted thin h-BN could improve the charge injection properties of TMD-based FETs by achieving ohmic contact behavior, even at low temperatures.[116] Instead of h-BN, similar effects could be delivered by inserting thiol molecules between the contact electrodes and MoS_2. Recently, simple contact engineering using the selective vapor deposition of thiol molecules was reported.[88] Thiol molecules tend to readily form covalent bonds with the sulfur vacancies of MoS_2, so thiol molecules selectively could be coupled only at the contact region (Figure 19a). As the result, the effective activation energies of thiol-treated FETs have shown significantly smaller values than those of untreated counterparts, as shown in Figure 19b. Consequently, the $I_{DS}-V_{DS}$ curves at the low-V_{DS} regime of thiol-treated FETs exhibited good linearity without an *S*-shape, which is typically evidenced in FETs with ohmic contact. The activation energy for the carrier injection can be dominantly determined by the characteristics of two barriers: the Schottky barrier and tunneling barrier. Especially, the tunneling behaviors are crucially affected by the tunneling barrier height and length. According to the recent work by Cho *et al.*, the activation energy for the hexadecanethiol (HDT)-treated MoS_2 FETs was slightly higher than those of DT- or PFDT-treated MoS_2 FETs.[89] Because both HDT and DT have the sulfur end-group, tunneling barrier would not be much different. However, the longer carbon chain length of HDT increases the tunneling length, resulting in slightly greater activation energy with lower tunneling probability. The inserted thiol molecules could eliminate the interfacial states that result in Fermi-level pinning and create additional tunneling paths, which could tailor the dominant carrier injection mechanism from thermionic emission to field emission. In a similar point of view, there is other research that has been conducted to achieve the lower contact resistance in TMD devices by improving the quality of vdW contact. To understand the contact properties of TMDs, it is necessary to consider the vdW gap formation which introduces the tunneling barrier

DOI: 10.1021/acsnano.9b02540
ACS Nano 2019, 13, 9713−9734

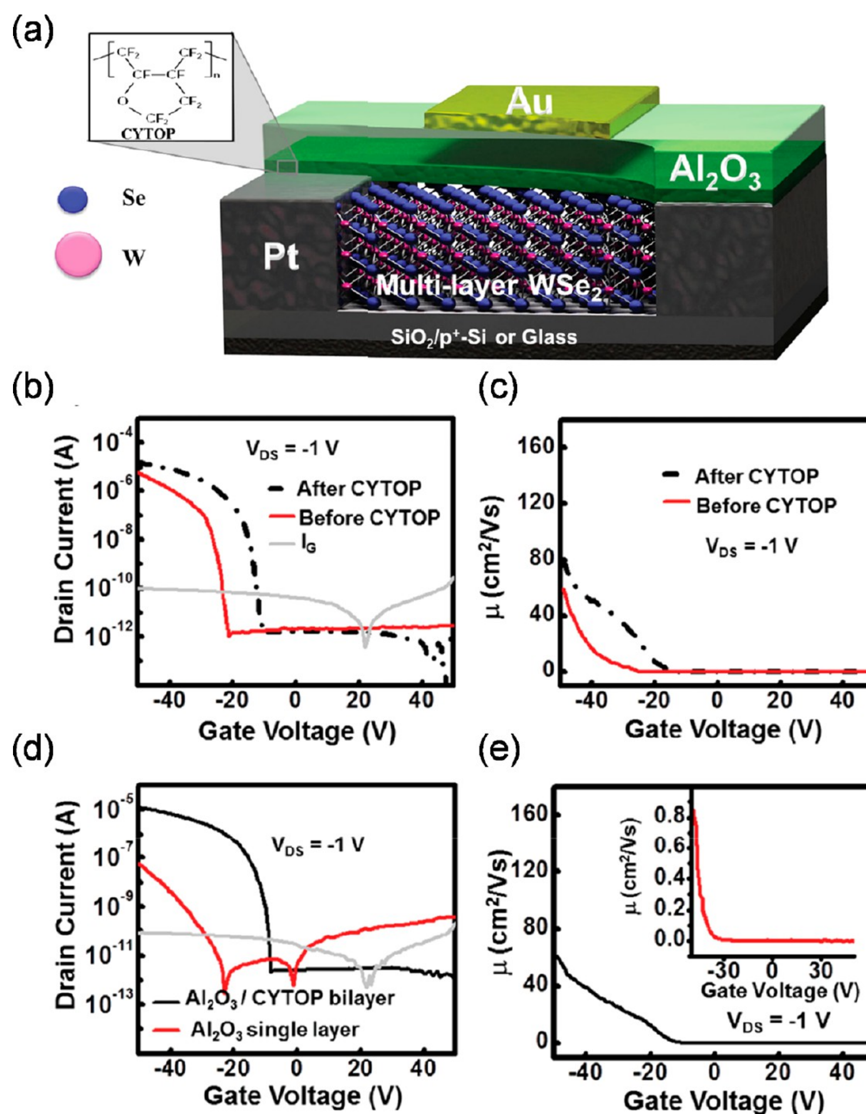

Figure 16. (a) Schematic 3D view to show the inside of the top-gate FET with the bilayer CYTOP/Al_2O_3 gate dielectric. (b, c) Transfer and mobility curves of a bottom-gate FET based on a 4L−WSe_2 flake. (d) The transfer curve of a 4L−WSe_2 bottom-gate FET with and without Al_2O_3/CYTOP bilayer passivation. (e) The mobility of a 4L−WSe_2 bottom-gate FET with Al_2O_3/CYTOP bilayer passivation. Inset: The mobility of the 4L−WSe_2 bottom-gate FET without the CYTOP buffer layer (Al_2O_3 passivation layer only). Reproduced with permission from ref 46. Copyright 2015 John Wiley & Sons, Inc.

between TMDs and metal electrodes. Liu *et al.* have reported that the high-energy metal deposition process can create considerable damages to the MoS_2 channel layer, introducing additional interfacial states which cause Fermi-level pinning effect.[124] In this manner, they transferred predeposited metal electrodes to the target MoS_2 flake to prevent physical damages from the high-energy deposition process. From this transfer method, they observed nearly ideal Schottky−Mott behavior, which conventional deposition methods for the electrode formation cannot achieve due to the high work function of Au. In addition, the creation of additional defects on the surface of MoS_2 was prevented by using the metal-transfer method, although the contact resistance and Schottky barrier height of Au electrode were found to be higher compared to the results in molecule-treated TMD devices. On the other hand, Wang *et al.* have reported the lowest contact resistance in single-layer MoS_2 FETs by delivering an ultraclean interface with indium (In) interlayers on MoS_2.[125] When they deposited a thin layer of In on MoS_2, any damages including lattice distortion and defects creation were not observed during the deposition process. Consequently, they obtained the lowest contact resistance in CVD grown NbS_2 FETs with In/Au electrodes. Also, the Schottky barrier height of MoS_2 FETs with In/Au electrode was found to be about 110 meV, and the activation energy of In/Au electrode was found be larger than that in the molecule-treated FETs. Although Cho *et al.*[89] did not report the extracted Schottky barrier height, we expect the contact-engineered MoS_2 devices with organic molecules would exhibit comparable values with Wang's and Liu's results with the consideration of the activation energies of the devices.

The attractive advantage of the use of organic molecules compared to the approaches reported by Liu *et al.*[124] and Wang *et al.*[125] is the wide versatility of modulation of the injection properties including the barrier height and injection mechanism by introducing various molecular moiety. For example, the injection properties could be modulated by changing molecular lengths and conductivity of molecular backbone as well as electric dipole moments. However,

DOI: 10.1021/acsnano.9b02540
ACS Nano 2019, 13, 9713−9734

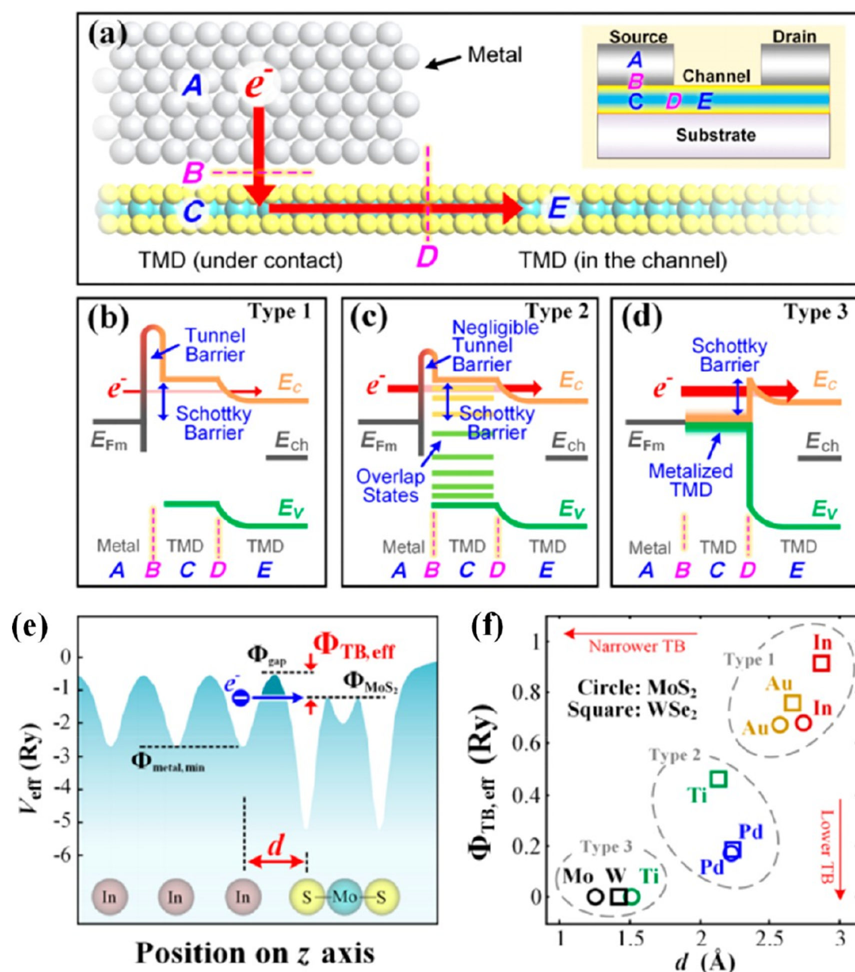

Figure 17. (a) Schematic cross-sectional view of a typical metal–MoS_2 contact (n-type top contact). A, C, and E denote the three regions, while B and D are the two interfaces separating them. Red arrows show the pathway (A → B → C → D → E) of electron injection from the contact metal (A) to the MoS_2 channel (E). The inset shows the source and drain contacts and the channel region in a typical backgated FET. (b–d) The three possible band diagrams of (a): metal contacts with (b) very weak bonding (type 1), (c) medium bonding (type 2), and (d) strong bonding (type 3). E_c, E_v, E_{Fm}, and E_{ch} represent the conduction band edge, valence band edge, metal Fermi level, and channel potential, respectively. (e) The plot of minimum effective potential (V_{eff}) *versus* z position for In-MoS_2 top contact. Φ_{MoS_2} is the V_{eff} of the Mo–S bond orbitals and, thereby, the effective tunnel barrier height ($\Phi_{TB;eff}$) is defined as the minimum barrier height that an electron from the metal has to overcome if it has the same potential energy as Φ_{MoS_2}. (f) The $\Phi_{TB;eff}$ *versus* d plot depending on the top contact material. Reproduced with permission from ref 111. Copyright 2014 American Physical Society.

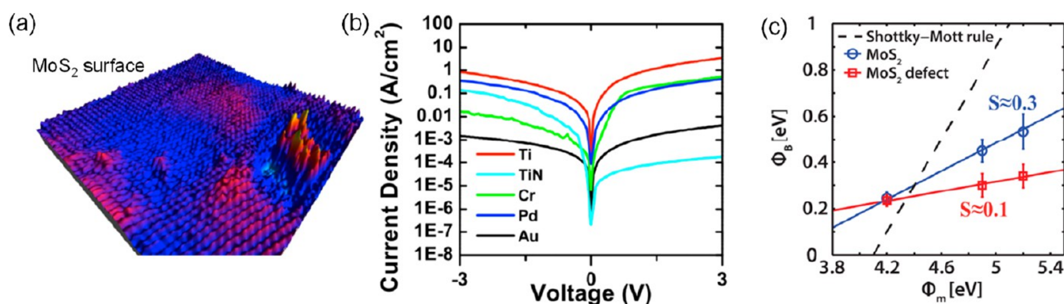

Figure 18. (a) A 3D image showing a high tunneling current from a defect of a 13.6 nm × 13.6 nm 3D STM image of the MoS_2 surface with atomic resolution acquired in negative bias. This image illustrates the higher conductivity of certain defects on the surface, which are attributed to metallic clusters. The imaging conditions were −100 mV, 0.5 nA. (b) The observed $I–V$ characteristics of the metal/MoS_2 contacts. Reproduced with permission from ref 33. Copyright 2014 American Chemical Society. (c) The Schottky barrier heights for the pristine MoS_2 (blue) and the defects (red) for different work functions of the tip (ϕ_M). The pinning S-factor and the charge neutrality level (ϕ_{CNL}) were extracted. The dotted line is the standard Schottky–Mott rule. Reproduced with permission from ref 121. Copyright 2017 American Chemical Society.

DOI: 10.1021/acsnano.9b02540
ACS Nano 2019, 13, 9713–9734

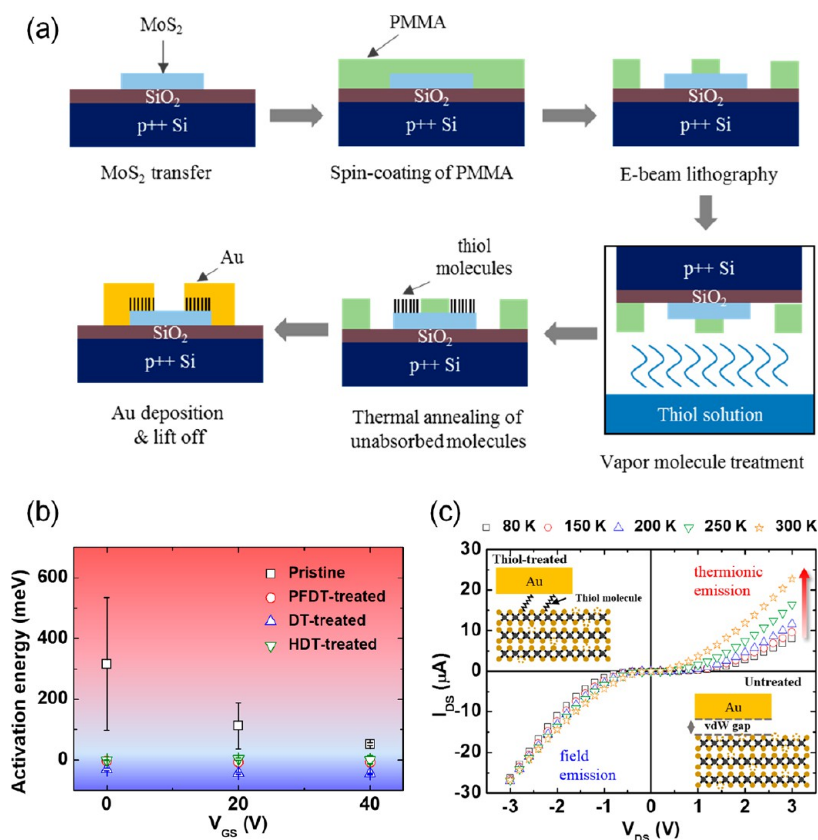

Figure 19. (a) Schematic images of the FET fabrication process. The thiol molecules were deposited only at the contact region by using a vapor deposition method. (b) The extracted activation energies of untreated, DT-treated, PFDT-treated, and HDT-treated MoS_2 FETs under different gate bias conditions. The red region represents "thermionic emission dominant", and the blue region represents "field emission dominant". (c) Output curves at different temperatures at a fixed gate bias. The drain electrode is DT treated, and the source electrode is untreated. The insets are the schematic images of the thiol-treated and the untreated contacts. Reproduced with permission from ref 89. Copyright 2018 John Wiley & Sons, Inc.

according to Cho *et al.*,[89] the weak nature of organic molecules under harsh environmental or operating conditions such as exposed to high temperature or high bias conditions could be a disadvantage compared to the previously reported results.

CONCLUSION AND OUTLOOK

For the past decade, TMDs have been intensively explored as an emerging semiconducting material, therefore, providing solid potential for use in the field of next-generation FETs. Due to their 2D nature, the implementation of ultrathin and transparent optoelectronics has been promised. Although significant efforts have been devoted to realizing high-performance TMD-based FETs and sensor applications by producing high-quality TMDs or introducing vdW heterostructures, further reliable approaches to control their electrical and optoelectronic characteristics from the device perspective should be given a higher priority for practical applications. In this review, we introduced recent progress in the interface engineering of TMDs in FET applications *via* modulating the electrical and optoelectronic characteristics by employing organic molecules and polymers. By using simple solution processing, including immersion, vapor deposition, and spin-coating, functionalized organic molecules and polymers can be adsorbed to coupling sites on TMDs, resulting in the engineered interfacial properties. In addition, undesirable surface defects, such as adatoms or vacancies, that degrade the electrical performance can be efficiently eliminated.

Herein, three promising avenues dependent on the dominant interfaces were classified into TMDs and air, TMDs and the dielectric, and TMDs and contacts and were systematically discussed. SCTD with organic molecules enables modulation of the electrical properties, such as the carrier concentration in TMD channels, as well as optoelectronic characteristics, including photodetectivity and photoresponsivity. The ability to facilely reversible de-dope provides great opportunities to engineer the performance of materials. Intrinsic defects located on the surface of TMDs can be passivated *via* simple treatments with polymers, such as PSS, or thiol-based molecules. It has been theoretically and experimentally determined that passivated TMDs exhibit a lower carrier concentration. At the interface between a TMD channel and dielectric layer, a SAM or grafted polymers, for example, end-functionalized PS, on the gate dielectric can suppress charge trapping and scattering, leading to better electrical performance of TMD FETs, including the on/off ratio, a lower *SS* value, and a smaller hysteresis window. At the interface between the TMD channel and *S*/*D* contacts, the introduction of organic molecules can dramatically improve the charge injection properties by reducing the activation energy *via* additional tunneling paths. Furthermore, Fermi-level pinning can be successfully suppressed by eliminating the interfacial states, which promises a reliable performance in FETs with metal−semiconductor interfaces. In addition, the ability to control the electrical and optoelectronic properties of TMDs

DOI: 10.1021/acsnano.9b02540
ACS Nano 2019, 13, 9713−9734

without physical or chemical damages is a great advantage in a viewpoint of realizing structurally sensitive 2D device applications. In other words, surface engineering with organic molecules and polymers allows non-invasive processing onto TMDs directly as well as gradually de-doping *via* a simple rinsing process with solvents. This potential can be a key pathway for realizing high-performance device applications. For example, the output performance of TMDs-based thermoelectrics could be improved by facilely modulating carrier type, carrier concentration, electrical conductivity, and thermal conductivity, which are key parameters for determining the energy conversion performance of thermoelectrics. Also, it will attract much interest in the field of spintronics, especially in spin valve devices which require exquisitely optimized contact resistance values resulting with a maximized magneto resistance ratio. In this manner, interface engineering with various compatible organic molecules and polymers having different lengths and conductivity of molecular backbone can be an attractive strategy for achieving optimal characteristics of TMDs.

However, further technological advancements should be achieved to substitute the mature semiconductors. For a better electrical performance and low-voltage operation, high-quality high-*k* dielectrics, such as h-BN, have to be used. Additionally, a critical bottleneck of organic materials, their weak nature under high-temperature or chemical processing, requires the more reliable strategies of interface engineering. From a manufacturing perspective, the scaling issue should be addressed with a high degree of design freedom, although many efforts have been examined, for example, the use of inkjet printing. The ultimate goal of this research would be the realization of ultrathin emerging optoelectronics based on TMD FETs and utilized in transparent and flexible systems operating with low-power consumption.

AUTHOR INFORMATION

Corresponding Authors

*E-mail: seungjun@kist.re.kr.

*E-mail: tlee@snu.ac.kr.

ORCID

Takhee Lee: 0000-0001-5988-5219

Notes

The authors declare no competing financial interest.

ACKNOWLEDGMENTS

The authors appreciate the support from the National Creative Research Laboratory Program (grant no. 2012026372) provided by the Ministry of Science and ICT of Korea. S.C. appreciates the support by the Korea Institute of Science and Technology (KIST) Future Resource Research Program (2E29520) and the National Research Foundation of Korea (NRF) grant funded by the Ministry of Science and ICT of Korea (NRF-2017R1C1B2002323).

VOCABULARY

self-assembled monolayer (SAM), the monolayer which is spontaneously composed of ordered molecular assemblies on the surface; **external quantum efficiency (EQE)**, the ratio of the number of carriers collected by the devices to the number of photons illuminated on the device from the external light source; **hopping transport**, charge transport mechanism when the charges transport between localized sites *via* tunneling or overcoming potential barriers; **phase engineering**, the engineering of the material phase which is typically used to refer a physically homogenous state of matter or crystal structure. For example, MoS_2 has two representative phases, semiconducting 2H phase (ABA stacked) and metallic 1T phase (ABC stacked); **activation energy**, the amount of energy needed to overcome energy barriers located between the metal−semiconductor contact region for charge carrier injection.

REFERENCES

(1) Ahmed, S.; Yi, J. Two-Dimensional Transition Metal Dichalcogenides and Their Charge Carrier Mobilities in Field-Effect Transistors. *Nano-Micro Lett.* **2017**, *9*, 50.

(2) Allain, A.; Kang, J.; Banerjee, K.; Kis, A. Electrical Contacts to Two-Dimensional Semiconductors. *Nat. Mater.* **2015**, *14*, 1195.

(3) Butler, S. Z.; Hollen, S. M.; Cao, L.; Cui, Y.; Gupta, J. A.; Gutiérrez, H. R.; Heinz, T. F.; Hong, S. S.; Huang, J.; Ismach, A. F.; Johnston-Halperin, E.; Kuno, M.; Plashnitsa, V. V.; Robinson, R. D.; Ruoff, R. S.; Salahuddin, S.; Shan, G.; Shi, L.; Spencer, M. G.; Terrones, M.; et al. Progress, Challenges, and Opportunities in Two-Dimensional Materials Beyond Graphene. *ACS Nano* **2013**, *7*, 2898−2926.

(4) Chhowalla, M.; Jena, D.; Zhang, H. Two-Dimensional Semiconductors for Transistors. *Nat. Rev. Mater.* **2016**, *1*, 16052.

(5) Ganatra, R.; Zhang, Q. Few-Layer MoS_2: A Promising Layered Semiconductor. *ACS Nano* **2014**, *8*, 4074−4099.

(6) Mas-Balleste, R.; Gomez-Navarro, C.; Gomez-Herrero, J.; Zamora, F. 2D Materials: To Graphene and Beyond. *Nanoscale* **2011**, *3*, 20−30.

(7) Radisavljevic, B.; Radenovic, A.; Brivio, J.; Giacometti, V.; Kis, A. Single-Layer MoS_2 Transistors. *Nat. Nanotechnol.* **2011**, *6*, 147.

(8) Wang, Q. H.; Kalantar-Zadeh, K.; Kis, A.; Coleman, J. N.; Strano, M. S. Electronics and Optoelectronics of Two-Dimensional Transition Metal Dichalcogenides. *Nat. Nanotechnol.* **2012**, *7*, 699.

(9) Xia, F.; Wang, H.; Xiao, D.; Dubey, M.; Ramasubramaniam, A. Two-Dimensional Material Nanophotonics. *Nat. Photonics* **2014**, *8*, 899.

(10) Kam, K. K.; Parkinson, B. A. Detailed Photocurrent Spectroscopy of The Semiconducting Group VIB Transition Metal Dichalcogenides. *J. Phys. Chem.* **1982**, *86*, 463−467.

(11) Mak, K. F.; Lee, C.; Hone, J.; Shan, J.; Heinz, T. F. Atomically Thin MoS_2: A New Direct-Gap Semiconductor. *Phys. Rev. Lett.* **2010**, *105*, 136805.

(12) Cai, L.; He, J.; Liu, Q.; Yao, T.; Chen, L.; Yan, W.; Hu, F.; Jiang, Y.; Zhao, Y.; Hu, T.; Sun, Z.; Wei, S. Vacancy-Induced Ferromagnetism of MoS_2 Nanosheets. *J. Am. Chem. Soc.* **2015**, *137*, 2622−2627.

(13) Kioseoglou, G.; Hanbicki, A. T.; Currie, M.; Friedman, A. L.; Gunlycke, D.; Jonker, B. T. Valley Polarization and Intervalley Scattering in Monolayer MoS_2. *Appl. Phys. Lett.* **2012**, *101*, 221907.

(14) Klinovaja, J.; Loss, D. Spintronics in MoS_2 Monolayer Quantum Wires. *Phys. Rev. B: Condens. Matter Mater. Phys.* **2013**, *88*, 075404.

(15) Mak, K. F.; McGill, K. L.; Park, J.; McEuen, P. L. The Valley Hall Effect in MoS_2 Transistors. *Science* **2014**, *344*, 1489−1492.

(16) Eichfeld, S. M.; Hossain, L.; Lin, Y.-C.; Piasecki, A. F.; Kupp, B.; Birdwell, A. G.; Burke, R. A.; Lu, N.; Peng, X.; Li, J.; Azcatl, A.; McDonnell, S.; Wallace, R. M.; Kim, M. J.; Mayer, T. S.; Redwing, J. M.; Robinson, J. A. Highly Scalable, Atomically Thin WSe_2 Grown *via* Metal−Organic Chemical Vapor Deposition. *ACS Nano* **2015**, *9*, 2080−2087.

(17) Jiao, L.; Liu, H. J.; Chen, J. L.; Yi, Y.; Chen, W. G.; Cai, Y.; Wang, J. N.; Dai, X. Q.; Wang, N.; Ho, W. K.; et al. Molecular-Beam Epitaxy of Monolayer $MoSe_2$: Growth Characteristics and Domain Boundary Formation. *New J. Phys.* **2015**, *17*, 053023.

(18) Lee, Y.-H.; Zhang, X.-Q.; Zhang, W.; Chang, M.-T.; Lin, C.-T.; Chang, K.-D.; Yu, Y.-C.; Wang, J. T.-W.; Chang, C.-S.; Li, L.-J.; Lin,

DOI: 10.1021/acsnano.9b02540
ACS Nano 2019, 13, 9713−9734

T.-W. Synthesis of Large-Area MoS_2 Atomic Layers with Chemical Vapor Deposition. *Adv. Mater.* **2012**, *24*, 2320−2325.
(19) Naylor, C. H.; Parkin, W. M.; Ping, J.; Gao, Z.; Zhou, Y. R.; Kim, Y.; Streller, F.; Carpick, R. W.; Rappe, A. M.; Drndic, M.; Kikkawa, J. M.; Johnson, A. T. C. Monolayer Single-Crystal 1T′-$MoTe_2$ Grown by Chemical Vapor Deposition Exhibits Weak Antilocalization Effect. *Nano Lett.* **2016**, *16*, 4297−4304.
(20) Schmidt, H.; Wang, S.; Chu, L.; Toh, M.; Kumar, R.; Zhao, W.; Castro Neto, A.; Martin, J.; Adam, S.; Özyilmaz, B.; Eda, G. Transport Properties of Monolayer MoS_2 Grown by Chemical Vapor Deposition. *Nano Lett.* **2014**, *14*, 1909−1913.
(21) Wang, X.; Feng, H.; Wu, Y.; Jiao, L. Controlled Synthesis of Highly Crystalline MoS_2 Flakes by Chemical Vapor Deposition. *J. Am. Chem. Soc.* **2013**, *135*, 5304−5307.
(22) Yue, R.; Barton, A. T.; Zhu, H.; Azcatl, A.; Pena, L. F.; Wang, J.; Peng, X.; Lu, N.; Cheng, L.; Addou, R.; McDonnell, S.; Colombo, L.; Hsu, J. W. P.; Kim, J.; Kim, M. J.; Wallace, R. M.; Hinkle, C. L. $HfSe_2$ Thin Films: 2D Transition Metal Dichalcogenides Grown by Molecular Beam Epitaxy. *ACS Nano* **2015**, *9*, 474−480.
(23) Late, D. J.; Liu, B.; Matte, H. S. S. R.; Dravid, V. P.; Rao, C. N. R. Hysteresis in Single-Layer MoS_2 Field Effect Transistors. *ACS Nano* **2012**, *6*, 5635−5641.
(24) Park, W.; Park, J.; Jang, J.; Lee, H.; Jeong, H.; Cho, K.; Hong, S.; Lee, T. Oxygen Environmental and Passivation Effects on Molybdenum Disulfide Field Effect Transistors. *Nanotechnology* **2013**, *24*, 095202.
(25) Yuan, S.; Roldán, R.; Katsnelson, M. I.; Guinea, F. Effect of Point Defects on The Optical and Transport Properties of MoS_2 and WS_2. *Phys. Rev. B: Condens. Matter Mater. Phys.* **2014**, *90*, 041402.
(26) Santosh, K.; Longo, R. C.; Addou, R.; Wallace, R. M.; Cho, K. Impact of Intrinsic Atomic Defects on The Electronic Structure of MoS_2 Monolayers. *Nanotechnology* **2014**, *25*, 375703.
(27) Bao, W.; Cai, X.; Kim, D.; Sridhara, K.; Fuhrer, M. S. High Mobility Ambipolar MoS_2 Field-Effect Transistors: Substrate and Dielectric Effects. *Appl. Phys. Lett.* **2013**, *102*, 042104.
(28) Chen, J.; Liu, B.; Liu, Y.; Tang, W.; Nai, C. T.; Li, L.; Zheng, J.; Gao, L.; Zheng, Y.; Shin, H. S.; Jeong, H. Y.; Loh, K. P. Chemical Vapor Deposition of Large-Sized Hexagonal WSe_2 Crystals on Dielectric Substrates. *Adv. Mater.* **2015**, *27*, 6722−6727.
(29) Guo, Y.; Wei, X.; Shu, J.; Liu, B.; Yin, J.; Guan, C.; Han, Y.; Gao, S.; Chen, Q. Charge Trapping at The MoS_2-SiO_2 Interface and its Effects on The Characteristics of MoS_2 Metal-Oxide-Semiconductor Field Effect Transistors. *Appl. Phys. Lett.* **2015**, *106*, 103109.
(30) Ilatikhameneh, H.; Ameen, T. A.; Klimeck, G.; Appenzeller, J.; Rahman, R. Dielectric Engineered Tunnel Field-Effect Transistor. *IEEE Electron Device Lett.* **2015**, *36*, 1097−1100.
(31) Illarionov, Y. Y.; Rzepa, G.; Waltl, M.; Knobloch, T.; Grill, A.; Furchi, M. M.; Mueller, T.; Grasser, T. The Role of Charge Trapping in MoS_2/SiO_2 and MoS_2/hBN Field-Effect Transistors. *2D Mater.* **2016**, *3*, 035004.
(32) Borghardt, S.; Tu, J.-S.; Winkler, F.; Schubert, J.; Zander, W.; Leosson, K.; Kardynał, B. E. Engineering of Optical and Electronic Band Gaps in Transition Metal Dichalcogenide Monolayers Through External Dielectric Screening. *Phys. Rev. Mater.* **2017**, *1*, 054001.
(33) McDonnell, S.; Addou, R.; Buie, C.; Wallace, R. M.; Hinkle, C. L. Defect-Dominated Doping and Contact Resistance in MoS_2. *ACS Nano* **2014**, *8*, 2880−2888.
(34) Liu, D.; Guo, Y.; Fang, L.; Robertson, J. Sulfur Vacancies in Monolayer MoS_2 and its Electrical Contacts. *Appl. Phys. Lett.* **2013**, *103*, 183113.
(35) Gong, C.; Colombo, L.; Wallace, R. M.; Cho, K. The Unusual Mechanism of Partial Fermi Level Pinning at Metal−MoS_2 Interfaces. *Nano Lett.* **2014**, *14*, 1714−1720.
(36) Zhou, Y.; Wang, Z.; Yang, P.; Zu, X.; Yang, L.; Sun, X.; Gao, F. Tensile Strain Switched Ferromagnetism in Layered NbS_2 and $NbSe_2$. *ACS Nano* **2012**, *6*, 9727−9736.
(37) Seifert, G.; Terrones, H.; Terrones, M.; Frauenheim, T. Novel NbS_2 Metallic Nanotubes. *Solid State Commun.* **2000**, *115*, 635−638.
(38) Ali, M. N.; Xiong, J.; Flynn, S.; Tao, J.; Gibson, Q. D.; Schoop, L. M.; Liang, T.; Haldolaarachchige, N.; Hirschberger, M.; Ong, N. P.; Cava, R. J. Large, Non-Saturating Magnetoresistance in WTe_2. *Nature* **2014**, *514*, 205.
(39) Brown, B. E. The Crystal Structures of WTe_2 and High-Temperature $MoTe_2$. *Acta Crystallogr.* **1966**, *20*, 268−274.
(40) Fang, H.; Chuang, S.; Chang, T. C.; Takei, K.; Takahashi, T.; Javey, A. High-Performance Single Layered WSe_2 p-FETs with Chemically Doped Contacts. *Nano Lett.* **2012**, *12*, 3788−3792.
(41) Sipos, B.; Kusmartseva, A. F.; Akrap, A.; Berger, H.; Forró, L.; Tutiš, E. From Mott State to Superconductivity in 1T-TaS_2. *Nat. Mater.* **2008**, *7*, 960.
(42) Lee, G.-H.; Yu, Y.-J.; Cui, X.; Petrone, N.; Lee, C.-H.; Choi, M. S.; Lee, D.-Y.; Lee, C.; Yoo, W. J.; Watanabe, K.; Taniguchi, T.; Nuckolls, C.; Kim, P.; Hone, J. Flexible and Transparent MoS_2 Field-Effect Transistors on Hexagonal Boron Nitride-Graphene Heterostructures. *ACS Nano* **2013**, *7*, 7931−7936.
(43) Kappera, R.; Voiry, D.; Yalcin, S. E.; Branch, B.; Gupta, G.; Mohite, A. D.; Chhowalla, M. Phase-Engineered Low-Resistance Contacts for Ultrathin MoS_2 transistors. *Nat. Mater.* **2014**, *13*, 1128.
(44) Wang, J.; Yao, Q.; Huang, C. W.; Zou, X.; Liao, L.; Chen, S.; Fan, Z.; Zhang, K.; Wu, W.; Xiao, X.; Jiang, C.; Wu, W.-W. High Mobility MoS_2 Transistor with Low Schottky Barrier Contact by Using Atomic Thick h-BN as a Tunneling Layer. *Adv. Mater.* **2016**, *28*, 8302−8308.
(45) Kiriya, D.; Tosun, M.; Zhao, P.; Kang, J. S.; Javey, A. Air-Stable Surface Charge Transfer Doping of MoS_2 by Benzyl Viologen. *J. Am. Chem. Soc.* **2014**, *136*, 7853−7856.
(46) Shokouh, S. H. H.; Jeon, P. J.; Pezeshki, A.; Choi, K.; Lee, H. S.; Kim, J. S.; Park, E. Y.; Im, S. High-Performance, Air-Stable, Top-Gate, p-Channel WSe_2 Field-Effect Transistor with Fluoropolymer Buffer Layer. *Adv. Funct. Mater.* **2015**, *25*, 7208−7214.
(47) Sim, D. M.; Kim, M.; Yim, S.; Choi, M.-J.; Choi, J.; Yoo, S.; Jung, Y. S. Controlled Doping of Vacancy-Containing Few-Layer MoS_2 *via* Highly Stable Thiol-Based Molecular Chemisorption. *ACS Nano* **2015**, *9*, 12115−12123.
(48) Schmidt, H.; Giustiniano, F.; Eda, G. Electronic Trnasport Properties of Transition Metal Dichalcogenide Field-Effect Devices: Surface and Interface Effects. *Chem. Soc. Rev.* **2015**, *44*, 7715−7736.
(49) Jariwala, D.; Marks, T. J.; Hersam, M. C. Mixed-Dimensional van der Waals Heterostructures. *Nat. Mater.* **2017**, *16*, 170−181.
(50) Bertolazzi, S.; Gobbi, M.; Zhao, Y.; Backes, C.; Samori, P. Molecular Chemistry Approaches for Tuning the Properties of Two-Dimensional Transition Metal Dichalcogenides. *Chem. Soc. Rev.* **2018**, *47*, 6845−6888.
(51) Hu, Z.; Wu, Z.; Han, C.; He, J.; Ni, Z.; Chen, W. Two-Dimensional Transition Metal Dichalcogenides: Interface and Defect Engineering. *Chem. Soc. Rev.* **2018**, *47*, 3100−3128.
(52) Lee, W. H.; Park, Y. D. Tuning Electrical Properties of 2D Materials by Self-Assembled Monolayers. *Adv. Mater. Interfaces* **2018**, *5*, 1700316.
(53) Wang, H.; Yuan, H.; Hong, S. S.; Li, Y.; Cui, Y. Physical and Chemical Tuning of Two-Dimensional Transition Metal Dichalcogenides. *Chem. Soc. Rev.* **2015**, *44*, 2664−2680.
(54) Zhang, X.; Shao, Z.; Zhang, X.; He, Y.; Jie, J. Surface Charge Transfer Doping of Low-Dimensional Nanostructures toward High-Performance Nanodevices. *Adv. Mater.* **2016**, *28*, 10409−10442.
(55) Zhao, Y.; Xu, K.; Pan, F.; Zhou, C.; Zhou, F.; Chai, Y. Doping, Contact and Interface Engineering of Two-Dimensional Layered Transition Metal Dichalcogenides Transistors. *Adv. Funct. Mater.* **2017**, *27*, 1603484.
(56) Cho, B.; Hahm, M. G.; Choi, M.; Yoon, J.; Kim, A. R.; Lee, Y.-J.; Park, S.-G.; Kwon, J.-D.; Kim, C. S.; Song, M.; Jeong, Y.; Nam, K.-S.; Lee, S.; Yoo, T. J.; Kang, C. G.; Lee, B. H.; Ko, H. C.; Ajayan, P. M.; Kim, D.-H. Charge-Transfer-Based Gas Sensing Using Atomic-Layer MoS_2. *Sci. Rep.* **2015**, *5*, 8052.
(57) Kufer, D.; Konstantatos, G. Highly Sensitive, Encapsulated MoS_2 Photodetector with Gate Controllable Gain and Speed. *Nano Lett.* **2015**, *15*, 7307−7313.

DOI: 10.1021/acsnano.9b02540
ACS Nano 2019, 13, 9713−9734

(58) Lee, G.-H.; Cui, X.; Kim, Y. D.; Arefe, G.; Zhang, X.; Lee, C.-H.; Ye, F.; Watanabe, K.; Taniguchi, T.; Kim, P.; Hone, J. Highly Stable, Dual-Gated MoS_2 Transistors Encapsulated by Hexagonal Boron Nitride with Gate-Controllable Contact, Resistance, and Threshold Voltage. *ACS Nano* **2015**, *9*, 7019−7026.

(59) Ma, j.; Choi, K.-Y.; Kim, S. H.; Lee, H.; Yoo, G. All Polymer Encapsulated, Highly-Sensitive MoS_2 Phototransistors on Flexible PAR Substrate. *Appl. Phys. Lett.* **2018**, *113*, 013102.

(60) Kang, D.-H.; Shim, J.; Jang, S. K.; Jeon, J.; Jeon, M. H.; Yeom, G. Y.; Jung, W.-S.; Jang, Y. H.; Lee, S.; Park, J.-H. Controllable Nondegenerate p-Type Doping of Tungsten Diselenide by Octadecyltrichlorosilane. *ACS Nano* **2015**, *9*, 1099−1107.

(61) Benjamin, C. J.; Zhang, S.; Chen, Z. Controlled Doping of Transition Metal Dichalcogenides by Metal Work Function Tuning in Phthalocyanine Compounds. *Nanoscale* **2018**, *10*, 5148−5153.

(62) Pak, J.; Jang, J.; Cho, K.; Kim, T.-Y.; Kim, J.-K.; Song, Y.; Hong, W.-K.; Min, M.; Lee, H.; Lee, T. Enhancement of Photodetection Characteristics of MoS_2 Field Effect Transistors Using Surface Treatment with Copper Phthalocyanine. *Nanoscale* **2015**, *7*, 18780−18788.

(63) Mouri, S.; Miyauchi, Y.; Matsuda, K. Tunable Photoluminescence of Monolayer MoS_2 *via* Chemical Doping. *Nano Lett.* **2013**, *13*, 5944−5948.

(64) Li, Y.; Xu, C.-Y.; Hu, P.; Zhen, L. Carrier Control of MoS_2 Nanoflakes by Functional Self-Assembled Monolayers. *ACS Nano* **2013**, *7*, 7795−7804.

(65) Du, Y.; Liu, H.; Neal, A. T.; Si, M.; Peide, D. Y. Molecular Doping of Multilayer MoS_2 Field-Effect Transistors: Reduction in Sheet and Contact Resistances. *IEEE Electron Device Lett.* **2013**, *34*, 1328−1330.

(66) Dey, S.; Matte, H. S. S. R.; Shirodkar, S. N.; Waghmare, U. V.; Rao, C. N. R. Charge-Transfer Interaction Between Few-Layer MoS_2 and Tetrathiafulvalene. *Chem. - Asian J.* **2013**, *8*, 1780−1784.

(67) Kang, D.-H.; Kim, M.-S.; Shim, J.; Jeon, J.; Park, H.-Y.; Jung, W.-S.; Yu, H.-Y.; Pang, C.-H.; Lee, S.; Park, J.-H. High-Performance Transition Metal Dichalcogenide Photodetectors Enhanced by Self-Assembled Monolayer Doping. *Adv. Funct. Mater.* **2015**, *25*, 4219−4227.

(68) Tarasov, A.; Zhang, S.; Tsai, M.-Y.; Campbell, P. M.; Graham, S.; Barlow, S.; Marder, S. R.; Vogel, E. M. Controlled Doping of Large-Area Trilayer MoS_2 with Molecular Reductants and Oxidants. *Adv. Mater.* **2015**, *27*, 1175−1181.

(69) Andleeb, S.; Kumar Singh, A.; Eom, J. Chemical Doping of MoS_2 Multilayer by p-Toluene Sulfonic Acid. *Sci. Technol. Adv. Mater.* **2015**, *16*, 035009.

(70) Ghimire, G.; Dhakal, K. P.; Neupane, G. P.; Jo, S. G.; Kim, H.; Seo, C.; Lee, Y. H.; Joo, J.; Kim, J. Optically Active Charge Transfer in Hybrids of Alq_3 Nanoparticles and MoS_2 Monolayer. *Nanotechnology* **2017**, *28*, 185702.

(71) Heo, K.; Jo, S.-H.; Shim, J.; Kang, D.-H.; Kim, J.-H.; Park, J.-H. Stable and Reversible Triphenylphosphine-Based n-Type Doping Technique for Molybdenum Disulfide (MoS_2). *ACS Appl. Mater. Interfaces* **2018**, *10*, 32765−32772.

(72) Peimyoo, N.; Yang, W.; Shang, J.; Shen, X.; Wang, Y.; Yu, T. Chemically Driven Tunable Light Emission of Charged and Neutral Excitons in Monolayer WS_2. *ACS Nano* **2014**, *8*, 11320−11329.

(73) Yoo, H.; Hong, S.; Moon, H.; On, S.; Ahn, H.; Lee, H.-K.; Kim, S.; Hong, Y. K.; Kim, J.-J. Chemical Doping Effects on CVD-Grown Multilayer $MoSe_2$ Transistor. *Adv. Electron. Mater.* **2018**, *4*, 1700639.

(74) Förster, A.; Gemming, S.; Seifert, G.; Tománek, D. Chemical and Electronic Repair Mechanism of Defects in MoS_2 Monolayers. *ACS Nano* **2017**, *11*, 9989−9996.

(75) Park, J. H.; Sanne, A.; Guo, Y.; Amani, M.; Zhang, K.; Movva, H. C. P.; Robinson, J. A.; Javey, A.; Robertson, J.; Banerjee, S. K.; Kummel, A. C. Defect Passivation of Transition Metal Dichalcogenides *via* a Charge Transfer van der Waals Interface. *Sci. Adv.* **2017**, *3*, No. e1701661.

(76) Qiu, H.; Xu, T.; Wang, Z.; Ren, W.; Nan, H.; Ni, Z.; Chen, Q.; Yuan, S.; Miao, F.; Song, F.; Long, G.; Shi, Y.; Sun, L.; Wang, J.; Wang, X. Hopping Transport Through Defect-Induced Localized States in Molybdenum Disulphide. *Nat. Commun.* **2013**, *4*, 2642.

(77) Song, S. H.; Joo, M.-K.; Neumann, M.; Kim, H.; Lee, Y. H. Probing Defect Dynamics in Monolayer MoS_2 *via* Noise Nanospectroscopy. *Nat. Commun.* **2017**, *8*, 2121.

(78) Zhou, W.; Zou, X.; Najmaei, S.; Liu, Z.; Shi, Y.; Kong, J.; Lou, J.; Ajayan, P. M.; Yakobson, B. I.; Idrobo, J.-C. Intrinsic Structural Defects in Monolayer Molybdenum Disulfide. *Nano Lett.* **2013**, *13*, 2615−2622.

(79) Tosun, M.; Chan, L.; Amani, M.; Roy, T.; Ahn, G. H.; Taheri, P.; Carraro, C.; Ager, J. W.; Maboudian, R.; Javey, A. Air-Stable n-Doping of WSe_2 by Anion Vacancy Formation with Mild Plasma Treatment. *ACS Nano* **2016**, *10*, 6853−6860.

(80) Bertolazzi, S.; Bonacchi, S.; Nan, G.; Pershin, A.; Beljonne, D.; Samorì, P. Engineering Chemically Active Defects in Monolayer MoS_2 Transistors *via* Ion-Beam Irradiation and Their Healing *via* Vapor Deposition of Alkanethiols. *Adv. Mater.* **2017**, *29*, 1606760.

(81) Zhang, X.; Liao, Q.; Liu, S.; Kang, Z.; Zhang, Z.; Du, J.; Li, F.; Zhang, S.; Xiao, J.; Liu, B.; Ou, Y.; Liu, X.; Gu, L.; Zhang, Y. Poly (4-Styrenesulfonate)-Induced Sulfur Vacancy Self-Healing Strategy for Monolayer MoS_2 Homojunction Photodiode. *Nat. Commun.* **2017**, *8*, 15881.

(82) Freeman, R. G.; Grabar, K. C.; Allison, K. J.; Bright, R. M.; Davis, J. A.; Guthrie, A. P.; Hommer, M. B.; Jackson, M. A.; Smith, P. C.; Walter, D. G.; Natan, M. J. Self-Assembled Metal Colloid Monolayers: An Approach to SERS Substrates. *Science* **1995**, *267*, 1629−1632.

(83) Love, J. C.; Estroff, L. A.; Kriebel, J. K.; Nuzzo, R. G.; Whitesides, G. M. Self-Assembled Monolayers of Thiolates on Metals as a Form of Nanotechnology. *Chem. Rev.* **2005**, *105*, 1103−1170.

(84) Prime, K. L.; Whitesides, G. M. Self-Assembled Organic Monolayers: Model Systems for Studying Adsorption of Proteins at Surfaces. *Science* **1991**, *252*, 1164−1167.

(85) Ulman, A. Formation and Structure of Self-Assembled Monolayers. *Chem. Rev.* **1996**, *96*, 1533−1554.

(86) Zhou, C.; Deshpande, M. R.; Reed, M. A.; Jones, L.; Tour, J. M. Nanoscale Metal/Self-Assembled Monolayer/Metal Heterostructures. *Appl. Phys. Lett.* **1997**, *71*, 611−613.

(87) Chen, X.; Berner, N. C.; Backes, C.; Duesberg, G. S.; McDonald, A. R. Functionalization of Two-Dimensional MoS_2: On the Reaction Between MoS_2 and Organic Thiols. *Angew. Chem., Int. Ed.* **2016**, *55*, 5803−5808.

(88) Cho, K.; Min, M.; Kim, T.-Y.; Jeong, H.; Pak, J.; Kim, J.-K.; Jang, J.; Yun, S. J.; Lee, Y. H.; Hong, W.-K.; Lee, T. Electrical and Optical Characterization of MoS_2 with Sulfur Vacancy Passivation by Treatment with Alkanethiol Molecules. *ACS Nano* **2015**, *9*, 8044−8053.

(89) Cho, K.; Pak, J.; Kim, J.-K.; Kang, K.; Kim, T.-Y.; Shin, J.; Choi, B. Y.; Chung, S.; Lee, T. Contact-Engineered Electrical Properties of MoS_2 Field-Effect Transistors *via* Selectively Deposited Thiol-Molecules. *Adv. Mater.* **2018**, *30*, 1705540.

(90) Li, Q.; Zhao, Y.; Ling, C.; Yuan, S.; Chen, Q.; Wang, J. Towards a Comprehensive Understanding of The Reaction Mechanisms Between Defective MoS_2 and Thiol Molecules. *Angew. Chem., Int. Ed.* **2017**, *56*, 10501−10505.

(91) Makarova, M.; Okawa, Y.; Aono, M. Selective Adsorption of Thiol Molecules at Sulfur Vacancies on $MoS_2(0001)$, Followed by Vacancy Repair *via* S−C Dissociation. *J. Phys. Chem. C* **2012**, *116*, 22411−22416.

(92) Nguyen, E. P.; Carey, B. J.; Ou, J. Z.; van Embden, J.; Gaspera, E. D.; Chrimes, A. F.; Spencer, M. J. S.; Zhuiykov, S.; Kalantar-zadeh, K.; Daeneke, T. Electronic Tuning of 2D MoS_2 Through Surface Functionalization. *Adv. Mater.* **2015**, *27*, 6225−6229.

(93) Peterson, S. L.; Schulz, K. H. Ethanethiol Decomposition Pathways on $MoS_2(0001)$. *Langmuir* **1996**, *12*, 941−945.

(94) Xu, B.; Su, Y.; Li, L.; Liu, R.; Lv, Y. Thiol-Functionalized Single-Layered MoS_2 Nanosheet as a Photoluminescence Sensing Platform *via* Charge Transfer for Dopamine Detection. *Sens. Actuators, B* **2017**, *246*, 380−388.

DOI: 10.1021/acsnano.9b02540
ACS Nano 2019, 13, 9713−9734

(95) Wiegenstein, C. G.; Schulz, K. H. Methanethiol Adsorption on Defective MoS_2(0001) Surfaces. *J. Phys. Chem. B* **1999**, *103*, 6913−6918.

(96) Yu, Z.; Pan, Y.; Shen, Y.; Wang, Z.; Ong, Z.-Y.; Xu, T.; Xin, R.; Pan, L.; Wang, B.; Sun, L.; Wang, J.; Zhang, G.; Zhang, Y. W.; Shi, Y.; Wang, X. Towards Intrinsic Charge Transport in Monolayer Molybdenum Disulfide by Defect and Interface Engineering. *Nat. Commun.* **2014**, *5*, 5290.

(97) Park, J.-M.; Cho, I.-T.; Kang, W.-M.; Park, B.-G.; Lee, J.-H. Elimination of The Gate and Drain Bias Stresses in I−V Characteristics of WSe_2 FETs by Using Dual Channel Pulse Measurement. *Appl. Phys. Lett.* **2016**, *109*, 053503.

(98) Cho, K.; Park, W.; Park, J.; Jeong, H.; Jang, J.; Kim, T.-Y.; Hong, W.-K.; Hong, S.; Lee, T. Electric Stress-Induced Threshold Voltage Instability of Multilayer MoS_2 Field Effect Transistors. *ACS Nano* **2013**, *7*, 7751−7758.

(99) Kwon, H.-J.; Jang, J.; Kim, S.; Subramanian, V.; Grigoropoulos, C. P. Electrical Characteristics of Multilayer MoS_2 Transistors at Real Operating Temperatures with Different Ambient Conditions. *Appl. Phys. Lett.* **2014**, *105*, 152105.

(100) Cheng, L.; Lee, J.; Zhu, H.; Ravichandran, A. V.; Wang, Q.; Lucero, A. T.; Kim, M. J.; Wallace, R. M.; Colombo, L.; Kim, J. Sub-10 nm Tunable Hybrid Dielectric Engineering on MoS_2 for Two-Dimensional Material-Based Devices. *ACS Nano* **2017**, *11*, 10243−10252.

(101) Chang, H.-Y.; Yang, S.; Lee, J.; Tao, L.; Hwang, W.-S.; Jena, D.; Lu, N.; Akinwande, D. High-Performance, Highly Bendable MoS_2 Transistors with High-*k* Dielectrics for Flexible Low-Power Systems. *ACS Nano* **2013**, *7*, 5446−5452.

(102) Ji, H.; Joo, M.-K.; Yun, Y.; Park, J.-H.; Lee, G.; Moon, B. H.; Yi, H.; Suh, D.; Lim, S. C. Suppression of Interfacial Current Fluctuation in $MoTe_2$ Transistors with Different Dielectrics. *ACS Appl. Mater. Interfaces* **2016**, *8*, 19092−19099.

(103) Radisavljevic, B.; Kis, A. Mobility Engineering and a Metal−Insulator Transition in Monolayer MoS_2. *Nat. Mater.* **2013**, *12*, 815.

(104) Yu, Z.; Ong, Z.-Y.; Pan, Y.; Cui, Y.; Xin, R.; Shi, Y.; Wang, B.; Wu, Y.; Chen, T.; Zhang, Y.-W.; Zhang, G.; Wang, X. Realization of Room-Temperature Phonon-Limited Carrier Transport in Monolayer MoS_2 by Dielectric and Carrier Screening. *Adv. Mater.* **2016**, *28*, 547−552.

(105) Cui, Y.; Xin, R.; Yu, Z.; Pan, Y.; Ong, Z.-Y.; Wei, X.; Wang, J.; Nan, H.; Ni, Z.; Wu, Y.; Chen, T.; Shi, Y.; Wang, B.; Zhang, G.; Zhang, Y.-W.; Wang, X. High-Performance Monolayer WS_2 Field-Effect Transistors on High-κ Dielectrics. *Adv. Mater.* **2015**, *27*, 5230−5234.

(106) Jeong, Y.; Park, J. H.; Ahn, J.; Lim, J. Y.; Kim, E.; Im, S. 2D $MoSe_2$ Transistor with Polymer-Brush/Channel Interface. *Adv. Mater. Interfaces* **2018**, *5*, 1800812.

(107) Chung, S.; Jang, M.; Ji, S.-B.; Im, H.; Seong, N.; Ha, J.; Kwon, S.-K.; Kim, Y.-H.; Yang, H.; Hong, Y. Flexible High-Performance All-Inkjet-Printed Inverters: Organo-Compatible and Stable Interface Engineering. *Adv. Mater.* **2013**, *25*, 4773−4777.

(108) Ha, J.; Chung, S.; Pei, M.; Cho, K.; Yang, H.; Hong, Y. One-Step Interface Engineering for All-Inkjet-Printed, All-Organic Components in Transparent, Flexible Transistors and Inverters: Polymer Binding. *ACS Appl. Mater. Interfaces* **2017**, *9*, 8819−8829.

(109) Najmaei, S.; Zou, X.; Er, D.; Li, J.; Jin, Z.; Gao, W.; Zhang, Q.; Park, S.; Ge, L.; Lei, S.; Kono, J.; Shenoy, V. B.; Yakobson, B. I.; George, A.; Ajayan, P. M.; Lou, J. Tailoring The Physical Properties of Molybdenum Disulfide Monolayers by Control of Interfacial Chemistry. *Nano Lett.* **2014**, *14*, 1354−1361.

(110) Li, S.-L.; Komatsu, K.; Nakaharai, S.; Lin, Y.-F.; Yamamoto, M.; Duan, X.; Tsukagoshi, K. Thickness Scaling Effect on Interfacial Barrier and Electrical Contact to Two-Dimensional MoS_2 Layers. *ACS Nano* **2014**, *8*, 12836−12842.

(111) Kang, J.; Liu, W.; Sarkar, D.; Jena, D.; Banerjee, K. Computational Study of Metal Contacts to Monolayer Transition-Metal Dichalcogenide Semiconductors. *Phys. Rev. X* **2014**, *4*, 031005.

(112) Pak, J.; Jang, Y.; Byun, J.; Cho, K.; Kim, T.-Y.; Kim, J.-K.; Choi, B. Y.; Shin, J.; Hong, Y.; Chung, S.; Lee, T. Two-Dimensional Thickness-Dependent Avalanche Breakdown Phenomena in MoS_2 Field-Effect Transistors under High Electric Fields. *ACS Nano* **2018**, *12*, 7109−7116.

(113) Cho, S.; Kim, S.; Kim, J. H.; Zhao, J.; Seok, J.; Keum, D. H.; Baik, J.; Choe, D.-H.; Chang, K. J.; Suenaga, K.; Kim, S. W.; Lee, Y. H.; Yang, H. Phase Patterning for Ohmic Homojunction Contact in $MoTe_2$. *Science* **2015**, *349*, 625−628.

(114) Chuang, S.; Battaglia, C.; Azcatl, A.; McDonnell, S.; Kang, J. S.; Yin, X.; Tosun, M.; Kapadia, R.; Fang, H.; Wallace, R. M.; Javey, A. MoS_2 p-Type Transistors and Diodes Enabled by High Work Function MoO_x Contacts. *Nano Lett.* **2014**, *14*, 1337−1342.

(115) Cui, X.; Shih, E.-M.; Jauregui, L. A.; Chae, S. H.; Kim, Y. D.; Li, B.; Seo, D.; Pistunova, K.; Yin, J.; Park, J.-H.; Choi, H.-J.; Lee, Y. H.; Watanabe, K.; Taniguchi, T.; Kim, P.; Dean, C. R.; Hone, J. C. Low-Temperature Ohmic Contact to Monolayer MoS_2 by van der Waals Bonded Co/h-BN Electrodes. *Nano Lett.* **2017**, *17*, 4781−4786.

(116) Das, S.; Chen, H.-Y.; Penumatcha, A. V.; Appenzeller, J. High Performance Multilayer MoS_2 Transistors with Scandium Contacts. *Nano Lett.* **2013**, *13*, 100−105.

(117) Kwon, H.; Choi, W.; Lee, D.; Lee, Y.; Kwon, J.; Yoo, B.; Grigoropoulos, C. P.; Kim, S. Selective and Localized Laser Annealing Effect for High-Performance Flexible Multilayer MoS_2 Thin-Film Transistors. *Nano Res.* **2014**, *7*, 1137−1145.

(118) Leong, W. S.; Luo, X.; Li, Y.; Khoo, K. H.; Quek, S. Y.; Thong, J. T. L. Low Resistance Metal Contacts to MoS_2 Devices with Nickel-Etched-Graphene Electrodes. *ACS Nano* **2015**, *9*, 869−877.

(119) Wang, L.; Meric, I.; Huang, P. Y.; Gao, Q.; Gao, Y.; Tran, H.; Taniguchi, T.; Watanabe, K.; Campos, L. M.; Muller, D. A.; Guo, J.; Kim, P.; Hone, J.; Shepard, K. L.; Dean, C. R. One-Dimensional Electrical Contact to a Two-Dimensional Material. *Science* **2013**, *342*, 614−617.

(120) Yang, R.; Zheng, X.; Wang, Z.; Miller, C. J.; Feng, P. X.-L. Multilayer MoS_2 Transistors Enabled by a Facile Dry-Transfer Technique and Thermal Annealing. *J. Vac. Sci. Technol., B: Nanotechnol. Microelectron.: Mater., Process., Meas., Phenom.* **2014**, *32*, 061203.

(121) Bampoulis, P.; van Bremen, R.; Yao, Q.; Poelsema, B.; Zandvliet, H. J. W.; Sotthewes, K. Defect Dominated Charge Transport and Fermi Level Pinning in MoS_2/Metal Contacts. *ACS Appl. Mater. Interfaces* **2017**, *9*, 19278−19286.

(122) Farmanbar, M.; Brocks, G. Controlling The Schottky Barrier at MoS_2/Metal Contacts by Inserting a BN Monolayer. *Phys. Rev. B: Condens. Matter Mater. Phys.* **2015**, *91*, 161304.

(123) Farmanbar, M.; Brocks, G. Ohmic Contacts to 2D Semiconductors Through van der Waals Bonding. *Adv. Electron. Mater.* **2016**, *2*, 1500405.

(124) Liu, Y.; Guo, J.; Zhu, E.; Liao, L.; Lee, S.-J.; Ding, M.; Shakir, I.; Gambin, V.; Huang, Y.; Duan, X. Approaching the Schottky-Mott Limit in van der Waals Metal-Semiconductor Junctions. *Nature* **2018**, *557*, 696−700.

(125) Wang, Y.; Kim, J. C.; Wu, R. J.; Martinez, J.; Song, X.; Yang, J.; Zhao, F.; Mkhoyan, A.; Jeong, H. Y.; Chhowalla, M. Van der Waals Contacts between Three-Dimensional Metals and Two-Dimensional Semiconductors. *Nature* **2019**, *568*, 70−74.

DOI: 10.1021/acsnano.9b02540
ACS Nano 2019, 13, 9713−9734